ELSEVIER

Chemical Geology 233 (2006) 309–327

CHEMICAL GEOLOGY
INCLUDING
ISOTOPE GEOSCIENCE

www.elsevier.com/locate/chemgeo

Asthenosphere–lithospheric mantle interaction in an extensional regime: Implication from the geochemistry of Cenozoic basalts from Taihang Mountains, North China Craton

Yan-Jie Tang *, Hong-Fu Zhang, Ji-Feng Ying

State Key Laboratory of Lithospheric Evolution, Institute of Geology and Geophysics, Chinese Academy of Sciences, P.O. Box 9825, Beijing 100029, PR China

Received 25 July 2005; received in revised form 27 March 2006; accepted 30 March 2006

Abstract

Compositions of Cenozoic basalts from the Fansi (26.3–24.3 Ma), Xiyang–Pingding (7.9–7.3 Ma) and Zuoquan (~5.6 Ma) volcanic fields in the Taihang Mountains provide insight into the nature of their mantle sources and evidence for asthenosphere–lithospheric mantle interaction beneath the North China Craton. These basalts are mainly alkaline (SiO_2=44–50 wt.%, Na_2O+K_2O=3.9–6.0 wt.%) and have OIB-like characteristics, as shown in trace element distribution patterns, incompatible elemental (Ba/Nb=6–22, La/Nb=0.5–1.0, Ce/Pb=15–30, Nb/U=29–50) and isotopic ratios ($^{87}Sr/^{86}Sr$=0.7038–0.7054, $^{143}Nd/^{144}Nd$=0.5124–0.5129). Based on TiO_2 contents, the Fansi lavas can be classified into two groups: high-Ti and low-Ti. The Fansi high-Ti and Xiyang–Pingding basalts were dominantly derived from an asthenospheric source, while the Zuoquan and Fansi low-Ti basalts show isotopic imprints (higher $^{87}Sr/^{86}Sr$ and lower $^{143}Nd/^{144}Nd$ ratios) compatible with some contributions of sub-continental lithospheric mantle. The variation in geochemical compositions of these basalts resulted from the low degree partial melting of asthenosphere and the interaction of asthenosphere-derived magma with old heterogeneous lithospheric mantle in an extensional regime, possibly related to the far effect of the India–Eurasia collision.

Keywords: Cenozoic basalt; Geochemistry; Asthenosphere; Lithospheric mantle; Extensional regime; North China Craton

1. Introduction

The North China Craton (NCC) was extensively thinned during the Late Mesozoic and Cenozoic, which resulted in the replacement of old, cold and depleted lithospheric mantle by young, hot and fertile mantle (Menzies et al., 1993; Griffin et al., 1998). The lines of evidence summarized in Griffin et al. (1998) include high surface heat flow, uplift and later basin development, slow seismic wave velocities in the upper mantle, and a change in the character of mantle xenoliths sampled by Paleozoic and Cenozoic volcanic rocks.

However, the mechanisms of such a lithospheric change beneath the craton have not been well understood. Menzies and Xu (1998) and Xu (2001) argued that the thermal–chemical erosion of the lithosphere could play an

* Corresponding author. Tel.: +86 10 62007821; fax: +86 10 62010846.
E-mail addresses: tangyangjie@mail.igcas.ac.cn (Y.-J. Tang), hfzhang@mail.igcas.ac.cn (H.-F. Zhang), jfying@mail.igcas.ac.cn (J.-F. Ying).

0009-2541/$ - see front matter © 2006 Elsevier B.V. All rights reserved.
doi:10.1016/j.chemgeo.2006.03.013

important role, which was perhaps triggered by circum-craton subduction and subsequent passive continental extension on the basis of Mesozoic basin development. Some studies further suggest a partial replacement and that the lithospheric mantle was stratified with old lithosphere underlain by newly accreted "oceanic-type" lithosphere (Fan et al., 2000; Zheng et al., 2001). Evidence from Mesozoic basalts and high-Mg basaltic andesites demonstrates that the Mesozoic lithospheric mantle was highly enriched in both incompatible elements and isotopic ratios, so it was distinct from both Paleozoic refractory and Cenozoic depleted lithospheric mantle (Zhang et al., 2002, 2003a, 2004; Fan et al., 2004). Its enrichment processes likely have been caused by interaction between melts of subducted or foundered crust and peridotites of lithospheric mantle (Zhang et al., 2002, 2004; Gao et al., 2004; Zhang, 2005), thereby linking the evolution of cratonic lithosphere with the formation of circum-craton orogenic belts.

It is worth noting that previous studies of the changing lithosphere are mainly based in the eastern NCC, i.e., the region east to the Daxing'anling–Taihang gravity lineament (Fig. 1b); little is known about Cenozoic lithospheric evolution in the region near the gravity lineament, other than studies of the Cenozoic Hannuoba basalts and their deep-seated xenoliths (Song and Fery, 1989; Song et al., 1990; Zhi et al., 1990; Basu et al., 1991; Tatsumoto et al., 1992; Gao et al., 2002; Xu, 2002; Zhou et al., 2002; Rudnick et al., 2004). Both thinning and thickening could occur beneath different parts of the NCC, since the Eastern Block of the NCC had lost most of its ancient lithospheric mantle whereas

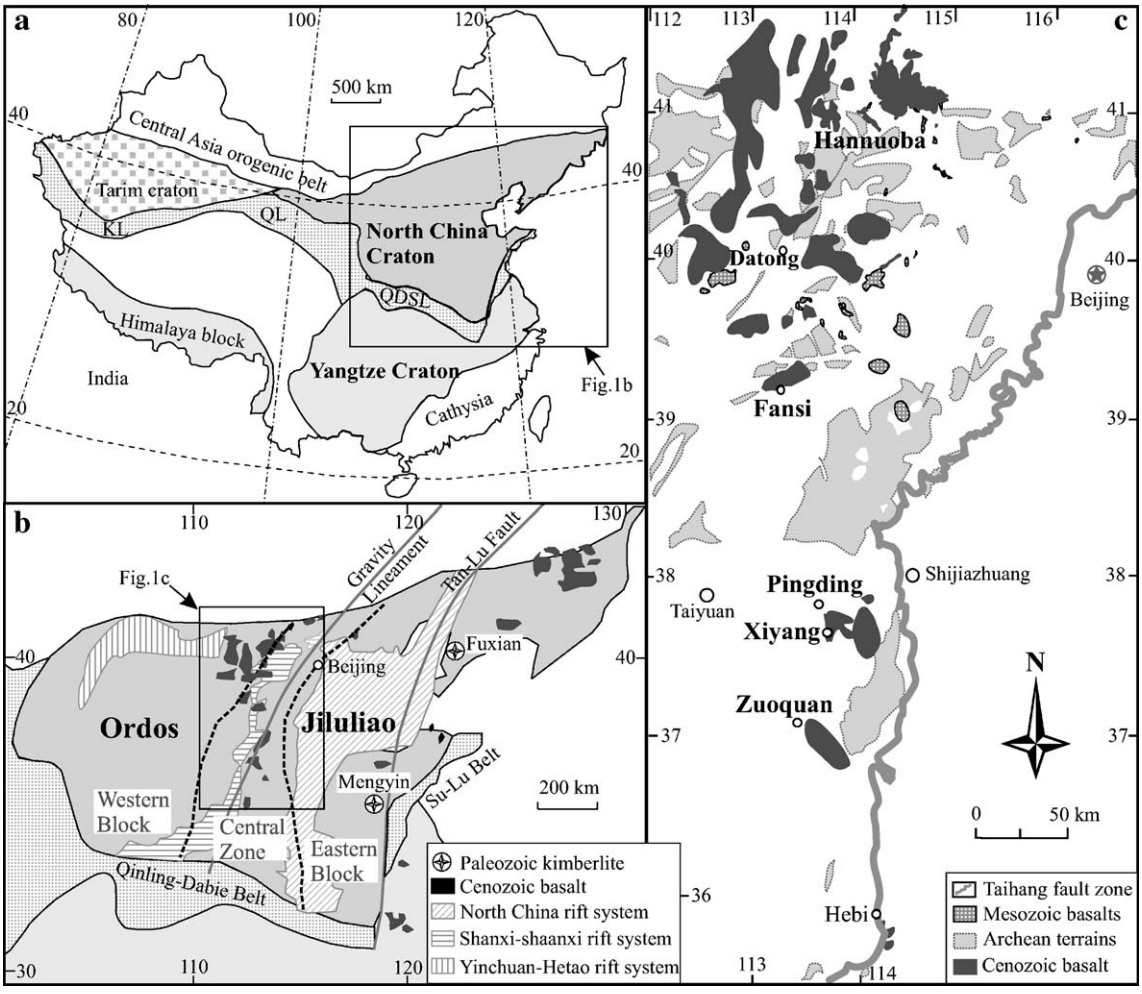

Fig. 1. (a) Simplified tectonic map showing major tectonic units of China (after Zhao et al., 2001). KL=Kunlun orogen; QL=Qilian orogen; QDSL=Qinling–Dabie–Sulu fold belt. (b) Three subdivisions of the North China Craton (after Zhao et al., 2000, 2001). Two dashed lines outline the Central Zone that separates the Western Block and Eastern Block. (c) Distribution of basalts in the Taihang Mountains (after Wu and Wang, 1978).

Table 1
K–Ar ages on whole rock powders of the basalts from the Taihang Mountains

Area	Sample	Weight (g)	K (%)	^{40}Ar total 10^{-11} (mol/g)	^{40}Ar radiogenic 10^{-11} (mol/g)	^{40}K 10^{-8} (mol/g)	Age ($\pm 2\sigma$) (Ma)
Fansi high-Ti	FS-1	0.01270	1.36	14.677	5.071	4.059	24.4±1.3
	FS-10	0.01299	1.56	14.197	7.026	4.656	25.8±0.9
	FS-32	0.01433	1.07	10.012	4.907	3.194	26.3±1.1
	HHL-1	0.01343	1.05	7.857	4.721	3.134	25.7±0.7
Fansi low-Ti	FS-2	0.01348	0.76	12.234	3.220	2.268	24.3±0.9
	FS-38	0.01451	1.43	8.643	6.230	4.268	25.0±0.5
Xiyang–Pingding	JX-1	0.01387	1.22	4.792	1.483	3.641	7.3±1.0
	MAS-2	0.01557	1.06	4.805	1.417	3.164	7.7±0.7
	JD-1	0.01312	1.44	4.231	1.980	4.298	7.9±0.6
Zuoquan	ZQ-1	0.01524	1.49	3.459	1.446	4.447	5.6±0.7

Parameters for ^{40}K: $\lambda_e = 0.581 \times 10^{-10}$ year^{-1}; $\lambda_{\hat{a}} = 4.962 \times 10^{-10}$ year^{-1}; ^{40}K = 0.01167 atom% (Steiger and Jager, 1977).

the Central Zone of the NCC (Fig. 1) still has considerable ancient lithosphere intact (Gao et al., 2002; Rudnick et al., 2006). Recently, Xu et al. (2004) reported on the geochemistry of the Cenozoic basalts from Datong and its adjacent regions, which has some implications for Cenozoic lithospheric thinning in the western NCC. The Taihang Mountains, situated in the Central Zone of the NCC (Fig. 1b), is the transition zone of lithospheric thickness. As a result, the lithospheric evolution beneath the Taihang Mountains is important for an overall understanding of the mechanism for lithospheric transformation beneath the NCC.

In this paper, we present K–Ar ages, major and trace elements, and Sr, Nd and Pb isotopic data for Cenozoic basalts from the Taihang Mountains. These data are interpreted in terms of petrogenesis, mantle source composition and its secular evolution, and asthenosphere–lithospheric mantle interaction.

2. Geologic background and petrology

The NCC is one of the world's oldest Archean cratons, preserving crustal remnants as old as 3800 Ma (Liu et al., 1992a). The Early Paleozoic Qilian orogen and the Late Paleozoic–Early Mesozoic Central Asia orogenic belt bound the craton to the west and the north, respectively, and in the south the Qinling–Dabie–Sulu high to ultrahigh-pressure metamorphic belt amalgamated the Craton with the Yangtze Craton (Fig. 1a). Two linear geological and geophysical zones, the Tan-Lu fault zone and Daxing'anling–Taihang gravity lineament crosscut the NCC. The gravity lineament separates the NCC into two blocks, the Ordos and Jiluliao (Fig. 1b).

Based on the geology and P–T–t paths of metamorphic rocks, the basement of the NCC is divided into three regions (Fig. 1b; Zhao et al., 2001): a Western Block, an Eastern Block and a Central Zone. The Western Block is a stable platform composed of Late Archean to Paleoproterozoic metasedimentary rocks unconformably overlying Archean basement. The latter mainly consists of granulite-facies gneisses and charnockite. The basement of the Eastern Block is mainly Archean orthogneisses. The Central Zone is composed of Late Archean amphibolites and granulites, which are overlain by Paleoproterozoic volcanic rocks, carbonate and sedimentary rocks (Zhao et al., 2001). These rocks underwent compressive deformation and metamorphism followed by rapid exhumation during Proterozoic time due to the collision between the Western and Eastern Blocks, which resulted in the amalgamation of the NCC.

The Eastern Block has a thin crust (<35 km), weakly negative to positive Bouguer gravity anomalies and high

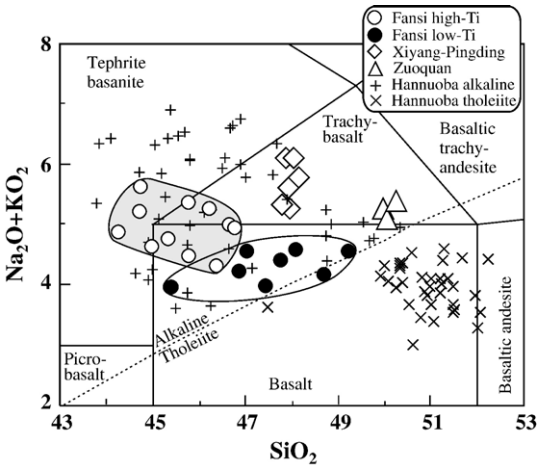

Fig. 2. Total alkali–silica diagram for the Cenozoic basalts. Previous data for Fansi and Hannuoba basalts are complied from Zhou and Armstrong (1982), Song et al. (1990), Zhi et al. (1990), Basu et al. (1991), Fan and Hooper (1991), Xie and Wang (1992), Liu et al. (1994), Xu et al. (2004). Classification of volcanic rocks is from Le Bas et al. (1986).

heat flow due to the continental extension during the Late Mesozoic and Cenozoic, leading to the NNE-trending North China rift system (Fig. 1b). Thus, the lithosphere is inferred to be thin (<80–100 km) under this block (Ma, 1989). The Western Block has a thick crust (>40 km), strong negative gravity anomalies and low heat flow,

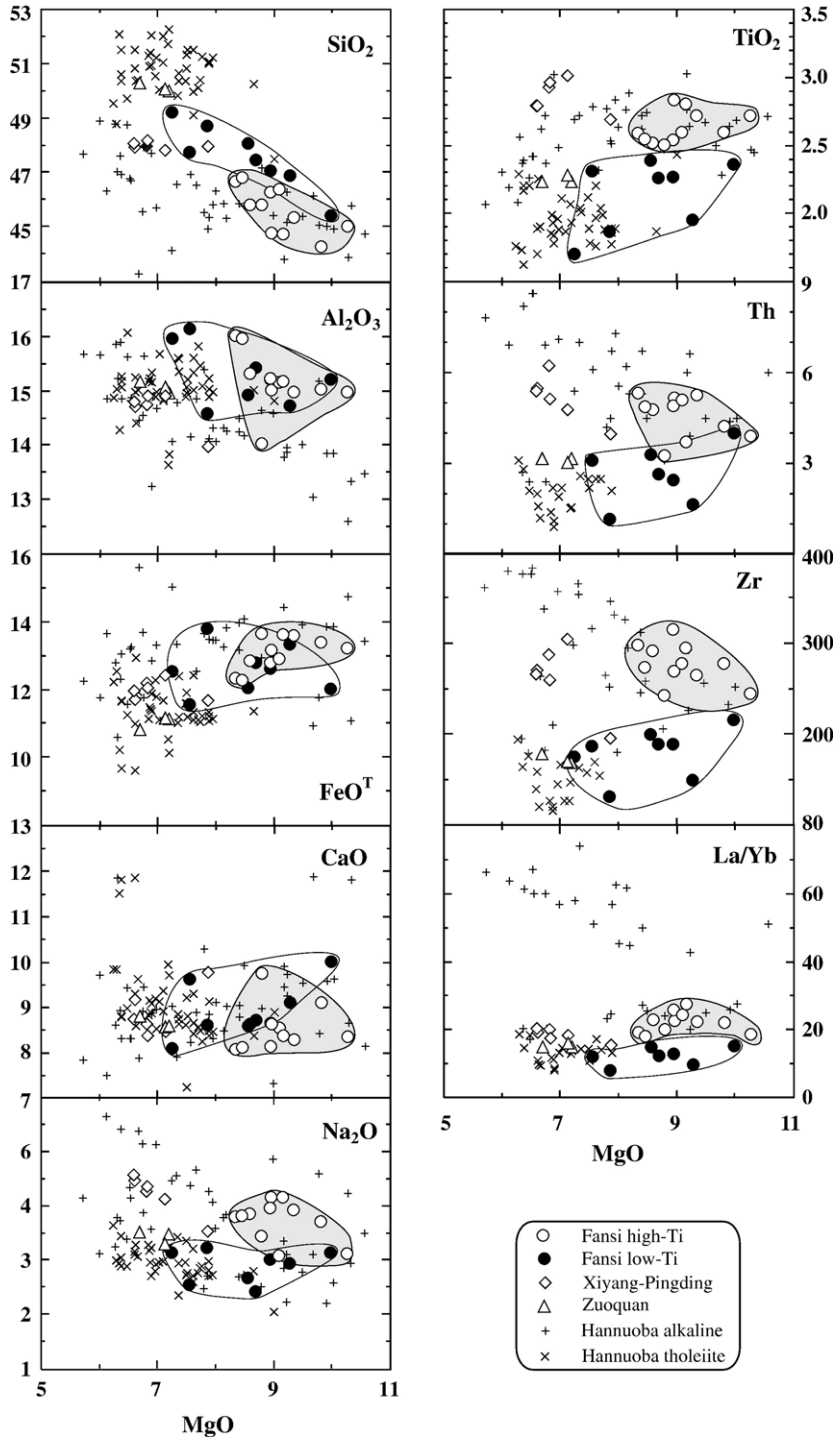

Fig. 3. Selected major (wt.%) and trace elements (ppm) vs. MgO diagrams. Major element contents are normalized to 100% on volatile-free basis.

Table 2
Major oxides (wt.%) and trace element concentrations (ppm) for the basalts from the Taihang Mountains

	Fansi high-Ti								Fansi low-Ti					Xiyang–Pingding						Zuoquan		
	FS-1	FS-8	FS-10	FS-30	FS-32	FS-33	HHL-1	HHL-2	FS-2	FS-3	FS-9	FS-36	FS-38	FHS-1	GB-2	JD-1	JX-1	JX-3	MAS-1	ZQ-1	ZQ-2	ZQ-4
SiO_2	44.07	44.28	44.13	43.53	45.20	43.96	45.41	45.73	47.01	47.06	44.81	46.31	46.91	47.70	47.31	47.03	47.40	46.51	47.21	49.80	49.78	50.13
TiO_2	2.79	2.44	2.65	2.63	2.38	2.52	2.52	2.49	2.34	2.28	2.33	2.21	2.26	2.68	2.89	2.74	2.91	2.93	2.74	2.22	2.27	2.22
Al_2O_3	14.78	14.80	14.58	14.47	14.88	14.70	15.58	15.60	14.59	15.90	14.99	15.06	15.16	13.90	14.55	14.44	14.66	14.51	14.54	14.90	14.97	15.13
$Fe_2O_3^T$	12.95	12.41	13.23	12.78	12.49	12.50	12.01	11.99	11.78	11.39	11.87	12.49	12.59	11.61	12.03	11.50	11.85	12.08	11.74	11.09	11.09	10.77
MnO	0.16	0.16	0.17	0.15	0.16	0.17	0.16	0.16	0.16	0.17	0.16	0.15	0.16	0.14	0.15	0.14	0.14	0.14	0.14	0.14	0.14	0.13
MgO	8.81	8.30	9.09	9.93	8.74	8.81	8.10	8.26	8.36	7.43	9.85	8.47	8.91	7.83	6.72	6.48	6.72	6.94	6.47	7.17	7.09	6.67
CaO	8.51	8.35	8.07	8.07	7.95	8.30	7.86	7.94	8.40	9.49	9.88	8.52	8.63	9.72	8.53	9.01	8.24	8.27	8.59	8.57	8.53	8.79
Na_2O	4.09	3.72	3.82	3.01	3.87	2.99	3.70	3.72	2.60	2.51	3.10	2.36	2.99	3.51	4.20	4.38	4.28	4.00	4.48	3.46	3.28	3.50
K_2O	1.47	1.48	0.83	1.48	1.28	0.96	1.18	1.10	1.90	1.83	0.82	1.55	1.59	1.74	1.34	1.61	1.41	1.19	1.51	1.79	1.78	1.87
P_2O_5	0.83	0.74	0.77	0.64	0.77	0.79	0.77	0.74	0.65	0.52	0.64	0.51	0.51	0.62	0.95	0.85	0.78	0.74	0.83	0.48	0.50	0.51
LOI	1.37	2.43	2.17	2.40	2.80	3.97	2.95	2.70	2.13	1.25	1.97	2.18	0.38	1.05	2.07	1.97	1.62	1.73	1.25	0.10	0.20	0.27
Total	99.8	99.1	99.5	99.1	100.5	99.7	100.2	100.4	99.9	99.8	100.4	99.8	100.1	100.5	100.7	100.1	100.0	99.0	99.5	99.7	99.6	100.0
Mg#[a]	61.6	61.2	61.8	64.6	62.2	62.4	61.4	61.8	62.5	60.6	66.1	61.5	62.5	61.3	56.8	57.0	57.2	57.5	56.5	60.4	60.1	59.3
La	42.0	40.6	40.6	31.9	44.8	42.3	39.5	37.0	30.0	27.4	34.2	25.3	24.7	33.6	31.8	27.3	34.8	35.2	39.0	23.1	23.5	24.9
Ce	89.8	88.8	85.6	68.1	97.8	89.0	83.3	77.9	66.0	60.8	74.3	54.8	54.1	70.5	66.3	56.9	71.5	73.0	81.4	48.9	50.1	51.4
Pr	11.0	10.9	10.3	8.5	11.9	10.6	9.68	9.12	8.02	7.61	9.26	6.87	6.72	8.66	8.14	7.07	8.78	8.96	10.1	6.19	6.36	6.49
Nd	46.1	44.7	42.3	35.4	49.0	43.3	39.1	37.1	32.1	33.4	38.3	29.4	28.3	37.6	36.5	31.8	39.3	39.2	43.3	26.6	27.1	28.1
Sm	9.53	9.56	8.66	8.08	10.2	8.66	7.90	7.46	7.03	6.78	7.98	6.10	6.31	9.15	8.46	7.24	8.95	8.93	10.08	6.17	6.43	6.38
Eu	3.02	2.81	2.67	2.41	3.08	2.76	2.48	2.32	2.60	2.19	2.53	2.12	2.05	2.83	2.72	2.32	2.83	2.88	3.12	2.09	2.08	2.15
Gd	8.38	8.24	7.80	6.96	8.84	7.90	7.27	7.10	7.01	6.91	7.51	6.35	6.17	8.42	8.50	7.10	8.64	8.70	9.60	6.16	5.98	6.17
Tb	1.28	1.15	1.12	1.07	1.22	1.14	1.05	0.99	1.00	0.99	1.05	0.95	0.93	1.24	1.21	1.05	1.24	1.24	1.36	0.86	0.93	0.96
Dy	6.07	5.32	5.43	5.35	5.64	5.57	5.47	5.13	5.62	5.54	5.50	4.91	4.84	6.26	6.16	5.68	6.35	6.23	6.60	4.67	4.88	4.76
Ho	1.04	0.94	0.96	0.90	0.98	1.02	0.99	0.92	0.95	0.98	1.06	0.91	0.87	1.12	1.06	0.93	1.07	1.07	1.08	0.81	0.82	0.89
Er	2.47	2.29	2.40	2.31	2.27	2.48	2.46	2.46	2.60	2.64	2.68	2.34	2.30	2.53	2.45	2.35	2.49	2.50	2.60	1.98	2.08	2.15
Tm	0.32	0.30	0.30	0.27	0.29	0.30	0.33	0.31	0.33	0.35	0.37	0.32	0.30	0.32	0.32	0.29	0.32	0.31	0.33	0.26	0.27	0.28
Yb	1.86	1.77	1.82	1.70	1.73	1.74	2.06	2.03	2.00	2.26	2.23	2.04	1.89	1.92	1.74	1.76	1.70	1.83	1.94	1.55	1.45	1.67
Lu	0.25	0.25	0.24	0.24	0.24	0.28	0.32	0.29	0.31	0.34	0.32	0.28	0.28	0.27	0.24	0.25	0.24	0.24	0.27	0.23	0.23	0.24
Y	20.2	20.0	21.0	19.4	21.4	21.9	22.4	21.2	20.0	21.1	21.9	20.2	19.8	25.0	24.2	22.1	24.6	24.6	25.6	18.6	19.0	19.9
Cs	0.45	0.54	0.43	0.34	0.56	0.51	0.48	0.43	0.44	0.42	0.48	0.32	0.21	0.53	0.50	0.26	0.46	0.43	0.54	0.33	0.28	0.24
Ba	539	590	562	431	642	572	600	587	621	633	602	471	422	514	447	408	465	460	468	449	445	463
Rb	16.5	36.8	19.3	12.3	16.0	60.1	28.3	29.0	18.0	17.4	24.5	13.5	12.6	10.1	9.7	22.6	17.8	31.9	6.9	22.9	22.8	26.6
Sr	947	934	911	779	1043	1095	1290	878	1104	1208	852	655	634	820	787	676	811	809	896	627	636	635
Nb	52.1	51.1	53.3	46.2	55.4	54.6	58.7	54.5	33.0	30.4	37.4	29.8	29.7	64.8	62.2	48.5	68.5	70.0	77.0	38.8	39.5	40.0
Ta	4.19	3.66	3.70	3.28	3.76	3.67	3.95	3.66	2.70	2.23	2.58	2.04	2.00	4.29	4.09	2.94	4.19	4.17	4.58	2.36	2.37	2.96
Zr	270	292	265	246	316	278	299	274	200	188	216	189	190	260	306	196	267	271	288	169	170	179
Hf	9.11	8.58	7.72	7.12	8.89	7.83	7.71	7.29	6.21	5.92	6.53	5.77	5.75	7.84	7.10	5.87	7.61	7.50	8.35	5.21	5.18	5.27
U	1.72	1.60	1.50	1.32	1.55	1.53	1.51	1.45	1.20	0.98	1.13	0.76	0.76	1.37	1.29	1.09	1.52	1.52	1.78	0.92	0.86	0.86
Th	5.16	4.79	5.25	3.90	4.91	5.10	5.33	4.88	3.32	3.11	4.01	2.65	2.46	5.14	4.78	3.97	5.39	5.47	6.22	3.16	3.05	3.16
Pb	3.45	3.45	3.61	2.69	3.58	3.50	4.12	3.70	3.20	3.12	3.19	2.53	2.52	2.43	2.19	2.30	3.08	2.91	3.17	2.95	2.41	2.70
Cr	160	188	178	199	189	148	131	137	144	116	266	201	249	165	212	242	150	123	146	231	243	222
Co	45.1	47.5	50.7	56.4	49.4	49.9	45.2	44.1	39.9	37.2	52.2	52.2	54.3	44.4	47.9	43.0	39.8	39.6	41.4	42.5	43.0	41.4
Ni	121	139	153	196	163	147	113	111	147	53	148	167	171	135	168	159	109	108	131	103	105	100
ΣREE	223	218	210	173	238	217	202	190	166	158	187	143	140	184	176	152	188	190	211	130	132	137
$(La/Yb)_N$	15.6	8.4	10.6	15.4	13.0	18.0	12.6	13.3	10.4	4.2	15.9	16.8	8.6	10.4	12.1	9.8	10.8	14.1	13.3	9.1	10.3	11.2

[a] $Mg\# = 100 \times Mg/(Mg+Fe)$ atomic ratio, assuming $FeO/Fe_2O_3^T = 0.85$.

reflecting a thick lithosphere (>100 km) (Ma, 1989). The Yinchuan–Hetao and Shanxi–Shaanxi rift systems formed in the Early Oligocene or Late Eocene, and their major extension developed in the Neogene and Quaternary (Ye et al., 1987; Ren et al., 2002). The Shanxi–Shaanxi rift system consists of many NE-trending en echelon grabens and exhibits a broad "S" shape (Fig. 1b).

In this study, fresh basalts were sampled from three localities along the Taihang Mountains, namely the Fansi, Xiyang–Pingding and Zuoquan basaltic fields (Fig. 1c). The K–Ar ages (Table 1) show that the Fansi basalts formed at 26.3–24.3 Ma (Oligocene) and the Xiyang–Pingding and Zuoquan basalts erupted at 7.9–7.3 Ma and ~5.6 Ma (Miocene), respectively.

The Fansi basalts cover ca. 550 km^2, with maximum thickness of 800 m (Wu and Wang, 1978). They have porphyritic texture and their phenocrysts (5–15 vol.%) are mainly olivine, clinopyroxene and orthopyroxene. The microgranular matrix is made up of olivine, clinopyroxene, orthopyroxene, plagioclase and magnetite. These basalts entrain abundant spinel–facies peridotitic xenoliths (up to 8 cm in diameter), whose average modal composition is olivine (69 vol.%), orthopyroxene (18 vol.%), clinopyroxene (11 vol.%) and spinel (2 vol.%), similar to those of xenoliths from eastern China (Fan et al., 2000). Pyroxenite and granulite xenoliths are very rare in these Fansi basalts, distinct from the Hannuoba locality, where abundant pyroxenite xenoliths exist.

The Xiyang–Pingding or Zuoquan basalts cover ca. 20 km^2, with an average thickness of 100 m (Wu and Wang, 1978). The Xiyang–Pingding basalts have olivine phenocrysts (5–10 vol.%) and xenocrysts (ca. 3 vol.%). The olivine xenocrysts (1–6 mm in diameter) have rounded shapes, kinked banding and compositional zonation. These features suggest that they are disaggregated minerals from old lithospheric mantle (Tang et al., 2004). Olivine phenocrysts are subhedral and fine-grained (0.5–1 mm in diameter). The microgranular matrix consists of plagioclase, olivine, augite and magnetite. Three samples were selected from the Zuoquan basalts to assess the spatial and temporal evolution of magmatism. They are generally fresh, with only slight iddingsitization of olivine. Their phenocrysts (10–20 vol.%) consist of

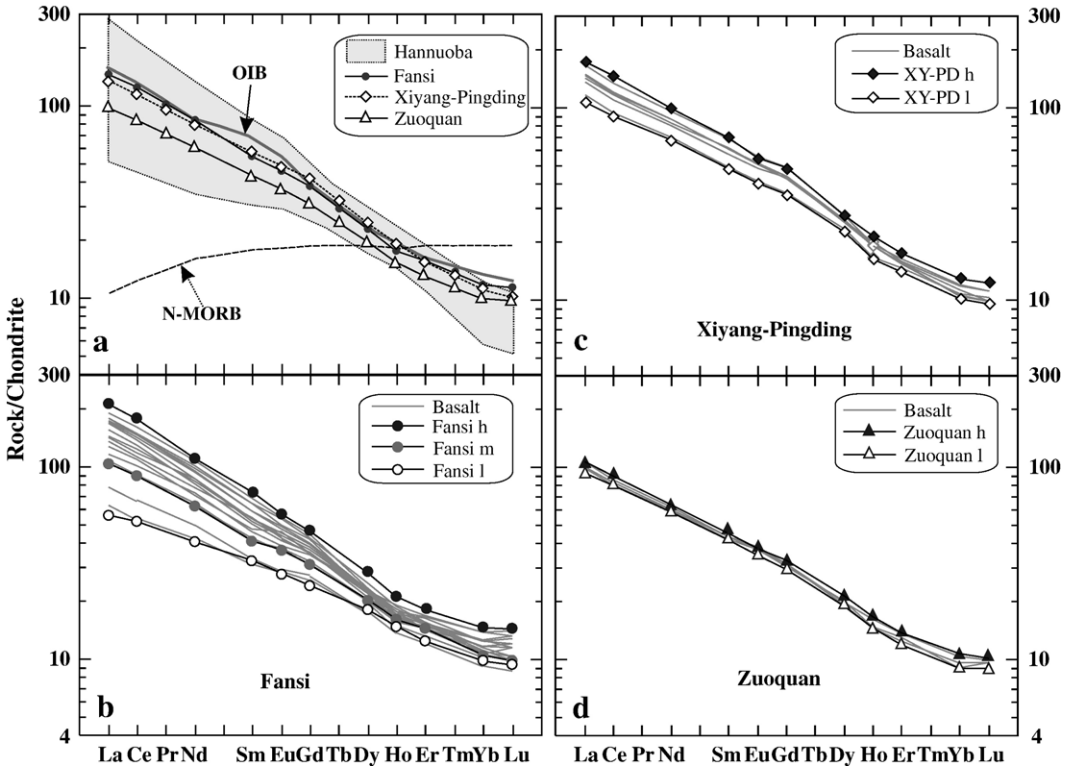

Fig. 4. Chondrite-normalized REE patterns for the Cenozoic basalts. Mean values of the REE for Fansi, Xiyang–Pingding and Zuoquan basalts (a). Non-modal batch melting models used to approach partial melts for Fansi (b), Xiyang–Pingding (c) and Zuoquan basalts (d). Normalization values are from Anders and Grevesse (1989). Data for N-MORB and OIB are from Sun and McDonough (1989); See Table 4 for model parameters.

plagioclase, olivine and augite; the matrix is made up of plagioclase, augite, magnetite and glass. Deep-seated xenoliths (peridotite or pyroxenite) are not found in Xiyang–Pingding or Zuoquan basalts.

3. Analytical methods

Whole-rock samples, after the removal of altered surfaces, were crushed to 60–80 mesh for dating. K–Ar ages were determined on a MM5400 mass spectrometer at the Research Institute of Petroleum Exploration and Development, China National Petroleum Co., following the procedure described by Fan et al. (2003).

For elemental and isotopic analyses, samples were ground in an agate mill to ~200 mesh. Major oxides were analyzed with a Phillips PW2400 X-ray fluorescence spectrometer at the State Key Laboratory of Lithospheric Evolution, Institute of Geology and Geophysics (IGG), Chinese Academy of Sciences. Fused glass disks were used and the analytical precisions were better than 5%, estimated from repeat analyses of GSR-3 (basalt, Chinese standard reference material, see Fan et al. (2004)). Trace element abundances were obtained on a VG-PQII ICP-MS at the IGG. Samples were dissolved in distilled $HF+HNO_3$ in 15 ml Savillex Teflon screw-cap beakers at 120 °C for 6 days, dried and then diluted to 50 ml for analysis. A blank solution was prepared and the total procedural blank was <50 ng for all trace elements. Indium was used as an internal standard to correct for matrix effects and instrument drift. Precision for all trace elements is estimated to be 5% and accuracy is better than 5% for most elements by analyses of the GSR-3 standard (Appendix A).

Sr, Nd and Pb isotopic compositions were measured on a Finnigan MAT-262 thermal ionization mass spectrometer at the IGG. The powders were washed with 0.3 N HCl for 1 h at ca. 100 °C, and dried after rinsing with purified water. The samples were weighed and spiked with mixed isotope tracers, dissolved in Teflon capsules with $HF+HNO_3$ at 120 °C for 7 days, and separated by cation-exchange techniques (Zhang et al., 2001). The mass fractionation corrections for Sr and Nd isotopic ratios were based on $^{86}Sr/^{88}Sr=0.1194$ and $^{146}Nd/^{144}Nd=0.7219$. Repeat analyses yielded $^{87}Sr/^{86}Sr$ of 0.710253 ± 0.000010 for the NBS-987 standard and $^{143}Nd/^{144}Nd$ of 0.511862 ± 0.000009 for the La Jolla standard. For Pb isotope analyses, the powders were dissolved in Teflon vials with purified HF at 120 °C for 6 days and then separated using anion-exchange columns (AG1×8, 200–400 mesh) with diluted HBr as an eluant. Repeat analyses of NBS981 yielded $^{206}Pb/^{204}Pb=16.916\pm0.009$, $^{207}Pb/^{204}Pb=15.461\pm0.010$, $^{208}Pb/^{204}Pb=36.616\pm0.012$. The Pb data were corrected based on the NBS981 recommended data. Detailed descriptions of the techniques are given in Zhang et al. (2002).

Table 3
Sr–Nd–Pb isotopic compositions for the Cenozoic basalts from Taihang Mountains

	Sample	$^{87}Rb/^{86}Sr$	$^{87}Sr/^{86}Sr$	2σ	$^{147}Sm/^{144}Nd$	$^{143}Nd/^{144}Nd$	2σ	ε_{Nd}	$^{206}Pb/^{204}Pb$	$^{207}Pb/^{204}Pb$	$^{208}Pb/^{204}Pb$
Fansi high-Ti	FS-1	0.0502	0.704097	10	0.1249	0.512795	9	3.26	17.414	15.433	37.806
	FS-8	0.1138	0.704254	15	0.1294	0.512747	7	2.34	17.932	15.452	37.924
	FS-10	0.0611	0.703993	14	0.1238	0.512755	8	2.51	17.815	15.453	37.853
	FS-30	0.0456	0.703826	13	0.1379	0.512796	10	3.27	17.907	15.461	37.887
	FS-32	0.0444	0.703880	11	0.1261	0.512731	10	2.05	17.901	15.432	37.839
	FS-33	0.1588	0.704268	12	0.1209	0.512750	10	2.43	17.758	15.434	37.741
	HHL-1	0.0635	0.704593	14	0.1222	0.512708	11	1.61	17.775	15.424	37.696
	HHL-2	0.0955	0.704163	13	0.1216	0.512733	11	2.10	17.709	15.415	37.652
Fansi low-Ti	FS-2	0.1067	0.705222	14	0.1555	0.512427	10	−3.99	17.415	15.354	37.606
	FS-3	0.0415	0.705385	13	0.1228	0.512540	8	−1.68	17.351	15.356	37.474
	FS-9	0.0831	0.704461	10	0.1260	0.512541	7	−1.67	17.629	15.433	37.699
	FS-36	0.0593	0.704322	12	0.1256	0.512634	8	0.15	17.362	15.379	37.459
	FS-38	0.0575	0.704231	10	0.1347	0.512600	9	−0.54	17.379	15.417	37.621
Xiyang–Pingding	JX-1	0.0354	0.703906	15	0.1471	0.512731	11	1.86	17.887	15.408	37.902
	JX-3	0.0358	0.703909	14	0.1403	0.512895	12	5.07	17.106	15.356	37.054
	FHS-1	0.0967	0.704171	14	0.1375	0.512689	12	1.05	17.291	15.339	37.687
	MAS-1	0.0634	0.703840	11	0.1378	0.512819	9	3.59	17.566	15.403	37.672
	JD-1	0.1139	0.703827	9	0.1378	0.512847	9	4.14	17.485	15.364	37.540
	GB-2	0.0221	0.704148	13	0.1408	0.512821	7	3.63	17.800	15.437	38.085
Zuoquan	ZQ-1	0.1057	0.704213	11	0.1402	0.512651	11	0.30	16.813	15.323	36.954
	ZQ-2	0.1039	0.704215	12	0.1435	0.512658	12	0.43	16.756	15.284	36.812
	ZQ-4	0.1210	0.704269	14	0.1370	0.512638	8	0.05	16.768	15.302	36.903

4. Results

4.1. Major oxides

4.1.1. Fansi basalts

Fansi basalts are dominantly alkaline and range from basanites to trachybasalts, with a few samples near the boundary between alkaline and tholeiite basalts (Fig. 2). The basalts generally have SiO_2 (44–49 wt.%) and alkalis (Na_2O+K_2O=3.9–5.6 wt.%, Fig. 2), similar to the Hannuoba alkaline basalts, with higher MgO (>8 wt.%) and Al_2O_3 (14.0–16.0 wt.%) contents (Fig. 3). Plots of MgO against major oxides show broadly negative correlations with SiO_2 and positive correlations with TiO_2. According to the content of TiO_2, the Fansi basalts can be divided into two groups, high-Ti (TiO_2>2.5 wt.

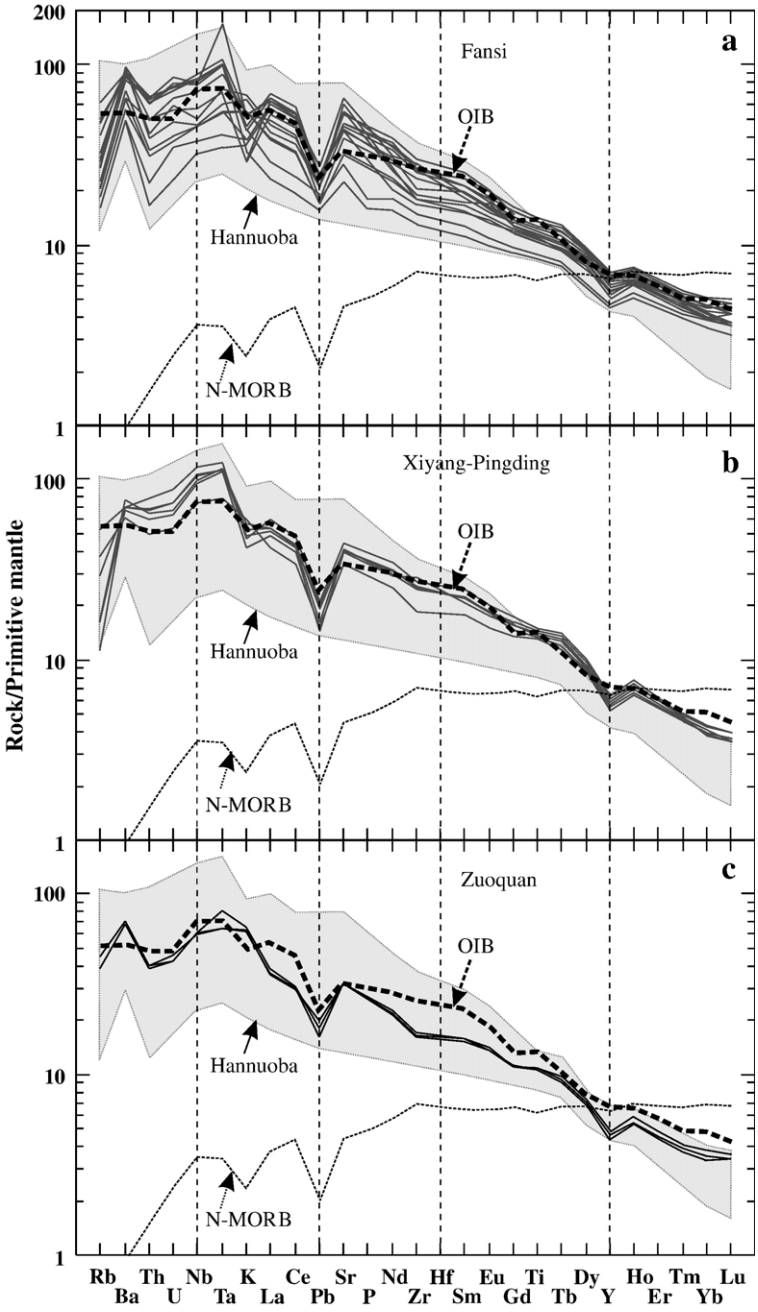

Fig. 5. Primitive mantle-normalized trace element diagrams for the Cenozoic basalts. The normalization values are from McDonough and Sun (1995).

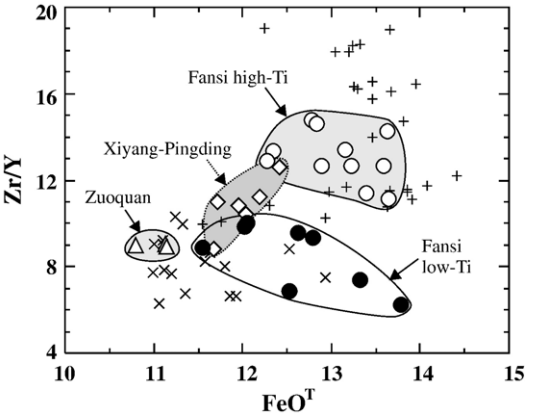

Fig. 6. Plot of Zr/Y vs. FeO^T (wt.%) for the Cenozoic basalts. N-MORB and OIB values are from Sun and McDonough (1989). Data sources are same as in Fig. 2 and symbols as in Fig. 3.

%) and low-Ti (TiO_2<2.5 wt.%). The high-Ti lavas have lower SiO_2, higher MgO and alkali contents than the low-Ti lavas (Fig. 3).

4.1.2. Xiyang–Pingding basalts

Xiyang–Pingding basalts are trachybasalts (Fig. 2) and have very small variations in SiO_2 contents (47–48 wt.%). They have high alkalis (Na_2O+K_2O=5.2–6.0 wt.%) and TiO_2 (2.7–3.0 wt.%) and low MgO (6.5–7.8 wt.%) contents (Fig. 3). Thus, these samples are all high-Ti basalts in terms of TiO_2 contents.

4.1.3. Zuoquan basalts

Zuoquan basalts are alkali olivine basalts. These lavas are close to the boundary between alkaline and tholeiite basalts, with some similarities to those of Hannuoba tholeiites in terms of SiO_2 and alkali contents (Fig. 2). They have high SiO_2 (~50 wt.%), low FeO^T (~11 wt.%), TiO_2 (2.2–2.3 wt.%) and MgO (~7 wt.%) contents (Table 2). These lavas are therefore low-Ti basalts.

4.2. Trace element geochemistry

All the basalts from the Taihang Mountains have very similar chondrite-normalized REE patterns in spite of slight differences in LREE/HREE fractionation (Fig. 4). They show LREE enrichment ($(La/Yb)_N$=10–18) and no Eu anomalies, which are typical of OIB and intraplate alkali basalts (Sun and McDonough, 1989; Wittke and Mack, 1993). The Fansi lavas have a relatively larger range in REE concentrations (ΣREE=140–238, Table 3). Xiyang–Pingding lavas have slightly lower contents of HREE than Fansi samples (Fig. 4a). The REE concentrations (ΣREE<137 ppm) for the Zuoquan basalts are generally lower than those of the Fansi and Xiyang–Pingding basalts. As a whole, these basalts have less LREE/HREE fractionation than the Hannuoba basalts.

In primitive mantle-normalized diagrams, all these basalts have LILE enrichments (Ba, Rb, Th, U, Sr) and negative Pb anomalies. They have no depletion in HFSE (Zr, Hf, Ti), but enrichment in Nb and Ta. These patterns are very similar to OIBs (Fig. 5). Incompatible element concentrations in Zuoquan basalts are below those of OIBs except for Ba, K and Ta (Fig. 5c). The highly incompatible element (Rb, Th) concentrations for these lavas scatter near OIB values.

The high-Ti and low-Ti basalts also show differences in Th and Zr contents, La/Yb ratios (Fig. 3), Zr/Y vs. FeO^T diagrams (Fig. 6), Ba/Nb vs. La/Nb and Nb/U vs. Ce/Pb diagrams (Fig. 7). Fansi high-Ti lavas have higher

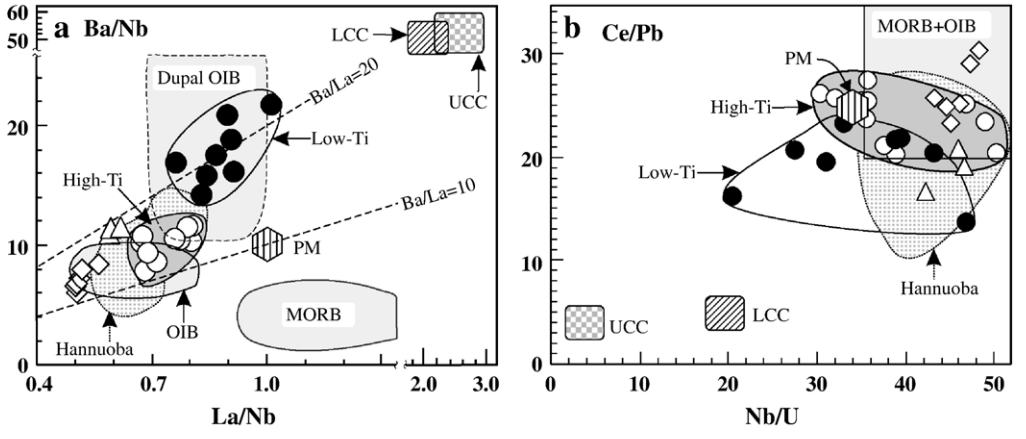

Fig. 7. La/Nb vs. Ba/Nb and Nb/U vs. Ce/Pb plots for the Cenozoic basalts. Data sources: PM, OIB, MORB and Dupal OIB (Sun and McDonough, 1989), Upper and lower continental crust (UCC and LCC) (Rudnick and Gao, 2003). Symbols as in Fig. 3.

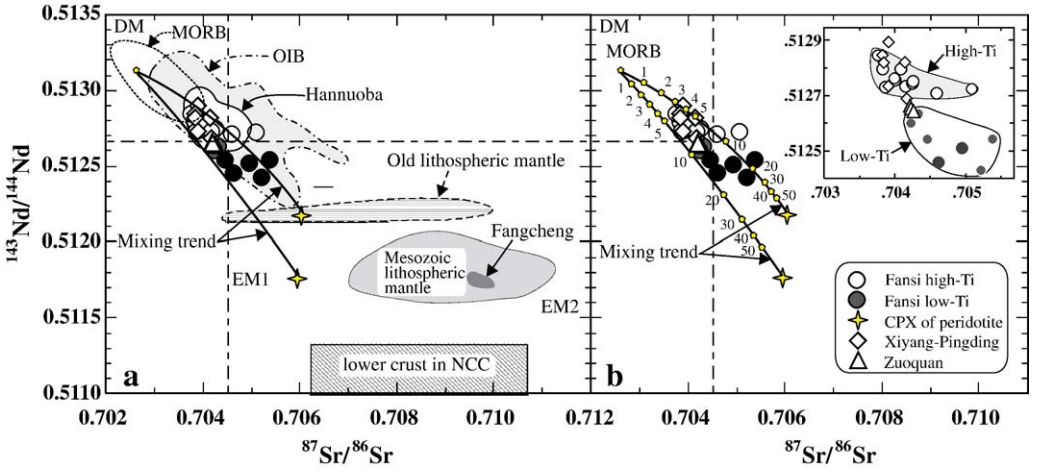

Fig. 8. $^{87}Sr/^{86}Sr$ vs. $^{143}Nd/^{144}Nd$ diagrams for the Cenozoic basalts from the Taihang Mountains, compared with the Hannuoba basalts (Song et al., 1990; Zhi et al., 1990; Basu et al., 1991; Xie and Wang, 1992), Cretaceous Fangcheng basalts, Mesozoic lithospheric mantle and old lithospheric mantle beneath the NCC (Zhang et al., 2002), lower crust of the NCC (Jahn et al., 1999), MORB, OIB, EM1 and EM2 (Zindler and Hart, 1986). Parameters for mixing trend: Sr (ppm), Nd (ppm), $^{87}Sr/^{86}Sr$ and $^{143}Nd/^{144}Nd$ are 20, 1.4, 0.70263, 0.51312 for asthenospheric melt (represented by N-MORB, Flower et al., 1998), 311, 12.4, 0.70604, 0.51219 and 142, 8.5, 0.70595, 0.51177 for old lithospheric mantle (represented by cpxs in two lherzolite xenoliths entrained in Fansi basalts, respectively). The numbers in Fig. b indicate the percentage of the contribution of old lithospheric mantle.

Th, Zr and Nb contents and La/Yb ratios. Their ratios of La/Nb (0.67–0.81), Nb/U (30–50) and Ce/Pb (20–27) are very close to those of OIB ($La/Nb_{OIB}=0.77$, $Nb/U_{OIB}=47$, $Ce/Pb_{OIB}=25$) (Sun and McDonough, 1989). High contents of highly incompatible elements (e.g. Th and Zr) in Fansi high-Ti and Xiyang–Pingding basalts may suggest that they were formed by relatively low degrees of partial melting of peridotitic mantle, while low-Ti lavas have lower Th, Zr (Fig. 3), Nb and Ce/Pb values, and higher La/Nb and Ba/Nb ratios (Fig. 7).

4.3. Sr, Nd and Pb isotopic ratios

In general, these basalts show a negative correlation between $^{143}Nd/^{144}Nd$ and $^{87}Sr/^{86}Sr$ (Fig. 8), and a linear array in $^{208}Pb/^{204}Pb$ vs. $^{206}Pb/^{204}Pb$ (Fig. 9a), generally parallel to the Northern Hemisphere Reference Line (Hart, 1984).

Fansi high-Ti and Xiyang–Pingding basalts have low Sr and high Nd isotopic ratios ($^{87}Sr/^{86}Sr=0.7038$–0.7051, $^{143}Nd/^{144}Nd=0.5127$–0.5129; Table 3), similar features to those of Hannuoba basalts and OIBs (Fig. 8). In contrast, Fansi low-Ti lavas have slightly higher Sr and lower Nd isotopic ratios. Pb isotopic ratios of Fansi high-Ti and Xiyang–Pingding lavas fall in the field for Hannuoba basalts and Indian MORB (Fig. 9). Zuoquan basalts have very restricted ranges in Sr and Nd isotopic compositions (Fig. 8), with some similarities to Fansi low-Ti basalts. Their very low $^{206}Pb/^{204}Pb$ ratios (~16.8, Fig. 9) distinguish them from other basalts

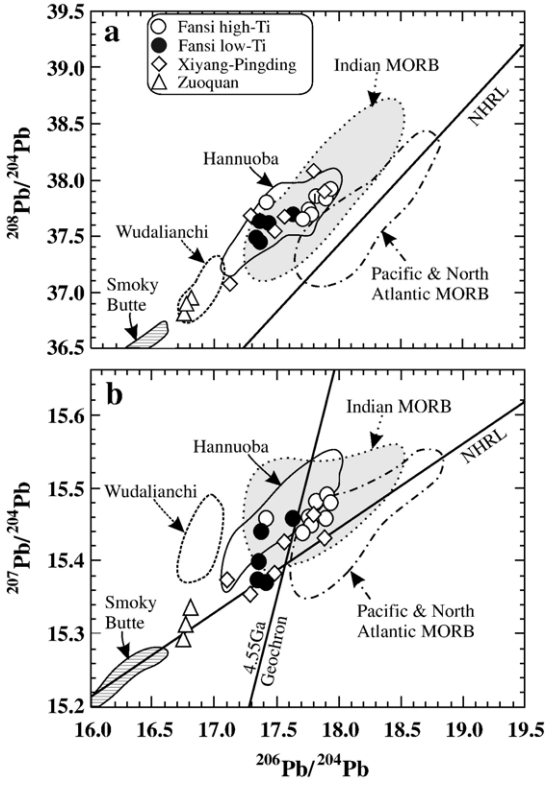

Fig. 9. $^{206}Pb/^{204}Pb$ vs. $^{208}Pb/^{204}Pb$ and $^{207}Pb/^{204}Pb$ diagrams for the Cenozoic basalts. Data sources: Indian MORB and Pacific and North Atlantic MORB (Barry and Kent, 1998; Zou et al., 2000), NHRL (Hart, 1984), Smoky Butte lamporites (Fraser et al., 1985) and Wudalianchi basalts (Zhang et al., 1998a; Zou et al., 2003).

from the Taihang Mountains, but they are close to the Smoky Butte lamproites and Wudalianchi potassic rocks (Zhang et al., 1998a; Zou et al., 2003), which suggest a long-term evolution in a low-μ environment (low U/Pb and high Th/U ratios), like the high-Mg basaltic andesites (Zhang et al., 2003a).

5. Discussion

5.1. Petrogenesis

5.1.1. Crustal contamination?

Cenozoic basalts from the NCC are mainly derived from asthenosphere with negligible crustal contamination (Zhou and Armstrong, 1982; Peng et al., 1986). For example, the geochemical compositions indicate that Hannuoba basalts were uncontaminated (e.g. Song et al., 1990; Basu et al., 1991; Xie and Wang, 1992). The Cenozoic basalts from Taihang Mountains have very similar geochemical features to those of Hannuoba basalts (Figs. 2–9) so suggesting that crustal contamination is insignificant. The occurrence of mantle xenoliths and xenocrysts suggests that the lavas ascended rapidly, implying that significant interaction with crustal wall rocks did not happen. Their clear OIB-like features in elemental ratios, e.g. high Ce/Pb, Nb/U, and low La/Nb, Ba/Nb, also suggest they are uncontaminated (Hofmann, 1988; Sun and McDonough, 1989) (Fig. 8). Furthermore, the contents of Ba (422–642 ppm) and Sr (627–1290 ppm) of these lavas are much higher than those of continental crust (Ba=259 ppm; Sr=348 ppm; Rudnick and Gao, 2003). Crustal assimilation coupled with fractional crystallization (AFC) is also unlikely, as this would result in progressive decreases in Cr, Ni, Co and Mg# with concomitant increase in $^{87}Sr/^{86}Sr$ ratios and decrease in $^{143}Nd/^{144}Nd$ ratios. These features are not observed in these samples (Tables 2 and 3). Thus, the compositions of these basalts can be used to probe their mantle sources.

5.1.2. Fractional crystallization

A few basalts with low and variable MgO (<8 wt.%), Ni (<200 ppm) and Cr contents (Table 2) might have experienced fractional crystallization of olivine and pyroxene. However in most lavas Ni and Cr do not display a clear trend with MgO, suggesting that fractional crystallization of minerals such as olivine and pyroxene is insignificant. Also, significant fractional crystallization of plagioclase could not occur because of the absence of an Eu anomaly (Fig. 4) and the correlation between Al_2O_3 and MgO (Fig. 3). Therefore, most of these basalts have the features of near primary magmas and their chemical compositions can be used to infer their geneses and mantle processes.

5.1.3. Magma origin: REE modeling of partial melting

Since these basalts experienced insignificant crustal contamination and fractional crystallization, their geochemical variations are likely to result mainly from the partial melting of mantle sources at different depths. Highly incompatible elemental ratios can be used to trace petrogenetic processes. For instance, the Zr/Y ratio generally remains constant during fractional crystallization, but varies during partial melting in basaltic systems (Nicholson and Latin, 1992). Zr is more incompatible than Y in the mantle, so Zr/Y ratios tend to be higher in small degree melts. Differences in FeO contents in primary magma could be related to the various depths and/or source compositions (Nicholson and Latin, 1992). Thus, high Fe and Zr/Y indicate high pressure and/or low degree of partial melting. The Fansi high-Ti basalts have high Zr/Y ratios (11–15) and FeO^T contents (12–14 wt. %), which overlap the Hannuoba alkaline basalts (Fig. 6). These features suggest that the high-Ti basalts were generated by low degrees of partial melting, similar to those of Hannuoba alkaline lavas. In contrast, Fansi low-Ti and Zuoquan lavas originated from slightly higher degrees of melting and/or a different mantle source for their low Zr/Y and FeO^T. The Xiyang–Pingding basalts, with intermediate Zr/Y ratios, might be produced from an intermediate degree of melting between that of the high-Ti and low-Ti basalts.

Relatively low HREE contents of all basalts (Yb_N= 8.9–13.9) indicate that garnet was present as a residual phase in their mantle sources. To verify this suggestion, the classic, non-modal batch melting equations of Shaw (1970) were used to model the REE patterns of these basalts with K_D values from Gorring and Kay (2001). Modeling parameters, mantle source composition, melt and source mode, and the degree of partial melting are listed in Table 4.

Between 1.1% and 6.0% partial melting of mantle source containing 4.5–7 wt.% garnet could account for the range of high- and low-concentration REEs in the Fansi basalts (Table 4, Fig. 4b). Results for the Xiyang–Pingding lavas indicate that their REE patterns are reproduced by 1.6% to 3.2% melting of a mantle source containing 4.5–6 wt.% garnet (Table 4, Fig. 4c). Similarly, 3.0% to 3.4% partial melting of mantle source containing 7–8 wt.% garnet could generate the REE patterns for the Zuoquan basalts (Table 4, Fig. 4d).

In summary, small degrees of partial melting of a garnet-bearing lherzolitic mantle source are required to explain the REE patterns observed in these basalts. The

Table 4
Model parameters and results of non-modal batch partial melting calculations (ppm) using various mineralogical and chemical compositions for diverse sources

Phase	Source mode							Melt mode	
	A1	A2	A3	B1	B2	C1	C2	M1	M2
Olivine	0.6	0.5	0.5	0.555	0.55	0.55	0.54	0.15	0.15
OPX	0.225	0.25	0.25	0.29	0.255	0.24	0.24	0.15	0.15
CPX	0.11	0.16	0.17	0.09	0.115	0.13	0.13	0.20	0.30
Spinel	0.02	0.02	0.01	0.02	0.02	0.01	0.01	0.20	0.20
Garnet	0.045	0.07	0.07	0.045	0.06	0.07	0.08	0.30	0.20

REE	Best fit to							Source
	Fansi h	Fansi m	Fansi l	XY-PD h	XY-PD l	Zuoquan h	Zuoquan l	
	1	2	3	4	5	6	7	S (S*)
La	51.56	24.78	12.97	40.37	23.30	23.98	21.64	0.8931
Ce	108.12	55.20	30.98	90.73	54.41	55.01	50.13	2.3075
Nd	47.73	27.68	18.39	44.95	29.98	29.15	27.10	1.7602
Sm	10.25	6.36	4.73	10.15	7.24	6.86	6.43	0.5772
Eu	3.10	1.98	1.55	3.09	2.27	2.12	1.98	0.2184
Gd	9.09	5.90	4.82	9.08	6.83	6.31	5.87	0.7748
Dy	7.45	4.98	4.37	6.90	5.34	5.24	4.83	0.9581 (0.8844)
Ho	1.35	0.91	0.83	1.25	0.97	0.94	0.86	0.2132 (0.1968)
Er	3.14	2.12	1.99	2.88	2.25	2.15	1.94	0.6240 (0.5760)
Yb	2.45	1.69	1.62	2.25	1.79	1.70	1.54	0.6409 (0.5916)
Lu	0.34	0.24	0.23	0.31	0.25	0.24	0.22	0.0962 (0.0888)

Degrees of melting and corresponding parameters

Melt No.	1	2	3	4	5	6	7
Source mode	A1	A2	A3	B1	B2	C1	C2
Melt mode	M1	M1	M1	M2	M2	M2	M2
Melting degree (%)	1.1	2.7	6.0	1.6	3.2	3.0	3.4
Mantle source	S	S	S	S*	S*	S	S

Symbols: XY-PD=Xiyang–Pingding; h=high-REE concentration; m=middle-REE concentration; l=low-REE concentration.

Sources: S: 1.3 times primitive mantle of Sun and McDonough (1989); S*: 1.3 times primitive mantle of Sun and McDonough (1989), except Dy, Ho, Er, Yb and Lu (1.2 ×). Source and melt mineralogy are taken arbitrary, but similar to those used in other partial melting calculations (Abdel-Rahmann, 2002; McKenzie and O'Nions, 1995). Modeling was performed using a spinel–garnet lherzolite mantle source assemblage with seven different modes. All mantle mineral phases are assumed to remain residual in the partially melted lherzolite since none of them is melted out at degrees of melting from 0.1% to 6%. Melt Nos. 1 to 7 are best-fit melts calculated by different degrees of batch partial melting.

systematic presence of garnet as a residual phase requires a melting depth in excess of 70–80 km, where garnet becomes stable. The results suggest a deeper origin for Zuoquan basalts, as the proportion of garnet becomes greater with increasing depth.

5.2. Mantle source and secular evolution

5.2.1. Implication from elemental compositions

The major and trace elemental compositions of these basalts resemble many alkali basalts from both oceanic and continental settings (Tu et al., 1991; Turner and Hawkesworth, 1995). Their incompatible trace element distribution patterns and ratios, such as Ba/Nb, La/Nb and Ce/Pb are generally OIB-like ((Figs. 4, 5, and 7)). The Nb/U ratio is relatively high and uniform in oceanic basalts (Hofmann et al., 1986; Hofmann, 1997). In contrast, many continental flood basalts have low Nb/U and Nb/La ratios. As Arndt and Christensen (1992) reported, since continental lithospheric mantle generally has negligible or positive Nb anomalies, the negative Nb anomalies in many continental flood basalts suggest that they could not be produced from direct melting of lithospheric mantle. Therefore, Nb fractionation may occur via melt-rock reaction during the passage of asthenospheric magma through the lithospheric mantle as a result of the different reaction rates of minerals in metasomatized peridotite (Arndt and Christensen, 1992). Although the OIB-like signature of our samples suggests an asthenospheric source, their variable Nb/U ratios (Fig. 7b) and a few slightly negative Nb anomalies (Fig. 5a) might indicate the involvement of the above fractionation process in their

origin. Thus, some low-Ti basalts with low Nb/U ratios might suggest an involvement of metasomatized lithospheric mantle in their source.

5.2.2. Implications of Sr, Nd and Pb isotopic ratios

The basalts from Taihang Mountains have very similar isotopic compositions (Figs. 8 and 9) to those of the Cenozoic Hannuoba basalts (Zhou and Armstrong, 1982; Peng et al., 1986; Song et al., 1990; Basu et al., 1991; Liu et al., 1994; Barry and Kent, 1998) and OIB, which are interpreted to have been derived from the asthenosphere.

The Sr and Nd isotopic compositions of Fansi high-Ti and Xiyang–Pingding basalts fall in the OIB field and overlap those of the Hannuoba basalts (Figs. 8 and 9), suggesting they originated from the upwelling asthenosphere. Fansi low-Ti lavas have lower $^{143}Nd/^{144}Nd$, $^{206}Pb/^{204}Pb$, but higher $^{87}Sr/^{86}Sr$ ratios than the high-Ti lavas, showing the imprints of old lithospheric mantle beneath the NCC. While the Sr–Nd isotopic ratios of Zuoquan basalts fall in the OIB field, their low Pb isotopic ratios (Fig. 9), approaching the fields for Smoky Butte lamproites and Wudalianchi potassic rocks, indicate their derivation from an ancient low-μ mantle source.

According to Zou et al. (2003), the low-μ Wudalianchi basalts are highly potassic and their source materials are dominantly phlogopite-bearing garnet peridotites. Because U is highly soluble and Th is relatively insoluble in subduction-related fluids, addition of such fluids into the mantle would produce ^{238}U-enriched magmas. Hence, Zou et al. (2003) proposed that a subducted slab might have lost fluids from subducted sediments before it was subducted into the deep mantle. Similarly, the low-μ source for the Zuoquan basalts might result from silicate melt metasomatism, perhaps relevant to the ancient subduction event in the central NCC at ~1.8 Ga (Zhao et al., 2001; Wang et al., 2004). This process has been recorded by the high-Mg# gabbroid rocks in southern Taihang Mountains (Wang et al., 2006).

The isotopic signature of Zuoquan basalts requires an ancient mantle source, metasomatized by an agent with lower Rb/Sr and U/Pb, but higher Sm/Nd ratios than the primitive mantle. High SiO_2 contents in Zuoquan basalts require that the agent was rich in silica. Thus the metasomatic agent could be silicate melt derived from the partial melting of subducted oceanic or continental crust during ancient subduction (Wang et al., 2006). Melts from phlogopite-bearing sources have high Rb/Sr (>0.1; Furman and Graham, 1999). However, the Zuoquan basalts have low Rb/Sr (<0.05), indicating an amphibole-bearing mantle source, consistent with the greater enrichment in Na_2O than K_2O in Zuoquan basalts. Due to the extremely low Pb isotopic ratios of lithospheric mantle, even small-scale involvement of such component would considerably lower the Pb isotopic ratios of Zuoquan basalts, but it is not the case for their Sr–Nd isotopic ratios. This can account for the low Pb isotopes in Zuoquan basalts. The fact that the Xiyang–Pingding lavas have different Pb isotopic ratios from those of Zuoquan, might suggest the heterogeneity of their mantle sources or different degrees of asthenosphere–lithospheric mantle interaction.

5.3. Asthenosphere–lithospheric mantle interaction

Mesozoic basalts (Fig. 8a) from the NCC have high $^{87}Sr/^{86}Sr$ and low $^{143}Nd/^{144}Nd$, and are depleted in HFSEs (Zhang et al., 2002, 2003a, 2004; Chen et al., 2004), whereas Cenozoic basalts display a depleted isotopic composition without HFSE anomalies (Xu et al., 1995; Xu, 2002). Magmas from the asthenosphere with some contributions of lithospheric mantle should have relatively higher Sr and lower Nd isotopic ratios than MORBs. This is particularly true for the early extension-related magmatism in rift systems. Therefore, the isotopic features demonstrate that the Cenozoic basalts from the Taihang Mountains were mainly derived from the asthenosphere, but small with variable degrees of contribution of lithospheric mantle. In contrast, contributions to the Fansi low-Ti and Zuoquan basalts were greater than those of Fansi high-Ti and Xiyang–Pingding basalts.

Based on mantle xenoliths (Tatsumoto et al., 1992; Fan et al., 2000; Chen et al., 2001; Xu, 2002; Zhou et al., 2002; Xu and Bodinier, 2004), the Cenozoic lithospheric mantle beneath the NCC is fertile in major oxides and depleted relative to primitive mantle character in Sr–Nd–Pb isotopic ratios. The old lithospheric mantle beneath the NCC has enriched Sr–Nd isotopic compositions (Fig. 8a, Tatsumoto et al., 1992; Zhang et al., 2002). Ancient lithosphere beneath the Central Zone of the NCC has been documented in mantle xenoliths by Re–Os studies (Gao et al., 2002; Zhi and Qin, 2004; Rudnick et al., 2006). However, these xenoliths do not have low $^{143}Nd/^{144}Nd$ and high $^{87}Sr/^{86}Sr$ ratios (Song and Fery, 1989; Rudnick et al., 2004; Xu et al., 2004). Clinopyroxene separates from two spinel lherzolite xenoliths entrained in Fansi basalts have enriched isotopic ratios ($^{87}Sr/^{86}Sr=0.70595$, $^{143}Nd/^{144}Nd=0.51177$ for FS-12, and $^{87}Sr/^{86}Sr=0.70604$, $^{143}Nd/^{144}Nd=0.51219$ for FS-26), close to the old lithospheric mantle beneath the NCC (Fig. 8). The mineral assemblages and compositions (Appendix B) and whole rock Os isotope data for Fansi xenoliths (Rudnick et al., 2006) are similar to those of

Hannuoba (~1.9 Ga Os isochron ages), confirming the persistence of the old lithospheric mantle beneath the Fansi locality.

The large differences in Sr–Nd isotopic ratios of peridotitic xenoliths between the Hannuoba and Fansi localities might be produced by peridotite–melt reaction proposed by Zhang (2006). Because of the small difference in the composition between asthenospheric basaltic melt (Fo ~ 89) and ancient mantle peridotites from the lithospheric mantle (Fo ~ 92), the decrease in Mg# produced by mantle peridotite–basaltic melt interaction is limited. Moreover, peridotite–melt interaction may not cause a large variation in Re–Os isotopic system of mantle peridotites due to the low Os concentrations of the percolating magmas (Reisberg et al., 2005), whereas the Nd and Sr isotopic ratios of the peridotites have been completely reset during the melt–rock reaction. The abundance of garnet-bearing pyroxenites in Hannuoba xenoliths indicate the presence of peridotite–melt reaction (Liu et al., 2005; Zhang, 2006). In contrast, Fansi peridotitic xenoliths have rare pyroxenite veins, indicating very limited peridotite–melt reaction.

As a result, the Fansi lherzolite xenoliths are believed to represent the old lithospheric mantle. Interaction of asthenospheric melts with such ancient lithospheric mantle may explain the basaltic magmatism. An asthenospheric source with minor involvement of old lithospheric mantle can thus account for the isotopic features of the basalts from Taihang Mountains (Fig. 8), consistent with the conclusion inferred from elemental results.

Using end-members defined by Sr and Nd elemental and isotopic ratios, two hypothetical mixing trends between asthenospheric melt (represented by N-MORB) (Flower et al., 1998) and old lithospheric mantle are shown in Fig. 8. The modeling reveals that the addition of 10–20% old lithospheric mantle component into asthenospheric melt will generate the observed Sr–Nd isotopic compositions for the Fansi low-Ti basalts and that the addition of 9–10% old component is required to generate the Zuoquan basalts.

5.4. Geodynamic implications

The Cenozoic basaltic magmatism in the Taihang Mountains can be correlated to the evolution of Himalaya–Tibetan orogen in terms of the spatial–temporal evolution of Cenozoic extensional regime, basaltic magmatism in eastern Tibet and North China, seismic tomography, and numerical modeling data. The lines of evidence for this are summarized below.

(1) The India–Asia collision commenced in the early Tertiary (Chung et al., 2005). According to the spatial–temporal variations of Cenozoic magmatism on the Tibetan plateau, Chung et al. (2005) proposed that only after the removal of the thickened Lhasa lithospheric root (~26 Ma) could the Indian lithosphere commence its northward underthrusting and hence serve as a pivotal control to the Himalaya–Tibetan orogenesis. The basalts in the Taihang Mountains erupted

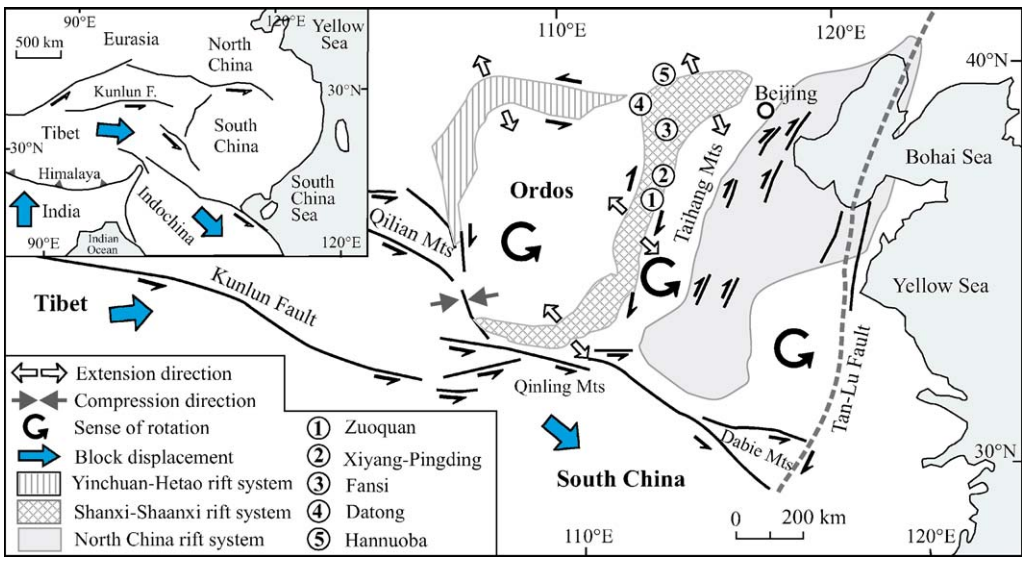

Fig. 10. Simplified map showing the extensional regime, block rotations and major active faults in North China and the eastern Tibet in the Cenozoic (modified from Tian et al., 1992; Zhang et al., 1998b, 2003b; Liu et al., 2004; Chung et al., 2005).

after ~26 Ma, a consequence of the northward underthrusting of the Indian lithosphere?

(2) The graben systems around the Ordos block, i.e. the Yinchuan–Hetao and Shanxi–Shaanxi graben systems (Figs. 1 and 10), occurred at the beginning of Cenozoic (Zhang et al., 2003b). They have been elongated by NW–SE-trending extension since the latest Miocene or earliest Pliocene, associated with counterclockwise rotation of blocks as a result of the push of Tibet through the left-lateral strike-slip fault system (Fig. 10; Zhang et al., 1998b, 2003b). Ren et al. (2002) deemed that the NW–SE-trending extensional stress field resulted from the rapid convergence of India–Eurasia relative to Pacific–Eurasia. Thus, the extensional regime in the Taihang Mountains is closely related to the India–Asia collision.

(3) Extension along pre-existing faults under the fold belt triggered asthenosphere upwelling, which led to the volcanism along the rift system. Liu et al. (2004) presented the evidence from P-wave travel time seismic tomography and numerical modeling, which shows that continuous low-velocity asthenospheric mantle extended from the Tibetan plateau to eastern China. Numerical simulations suggest that the Indo-Asian collision has driven significant lateral extrusion of the asthenospheric mantle, leading to diffusive asthenospheric upwelling, rifting, and widespread Cenozoic volcanism in eastern China (Liu et al., 2004).

(4) Fansi basalts are the same age as Hannuoba basalts and show many compositional features of the Hannuoba basalts (Liu et al., 1992b). As a whole, they have ages older than those of Zuoquan and Xiyang–Pingding lavas, indicating that the Himalaya–Tibetan orogen play an important role in the Taihang basaltic magmatism because the counterclockwise rotation of Ordos block may produce initial extension and rifting in the northern North China Craton. Consequently, the basalts erupted earlier in the north than in the center of this craton.

(5) Is there any contribution from the subduction of the Pacific plate during Cenozoic? Recent U–Th disequilibrium data for the potassic basalts from northeast China argue against the contribution from the Pacific plate (Zou et al., 2003). Since the Taihang Mountains are even further away from the Pacific subduction zone, and no material contribution from the Pacific subduction has apparently been observed in the Cenozoic magmatism (Zhou and Armstrong, 1982; Fan and Hooper, 1991; Liu et al., 1994; Zou et al., 2003; Xu et al., 2005), Pacific subduction may not play a major role in the generation of the basalts from the Taihang Mountains.

5.5. Lithospheric thickness and thinning mechanism

The REE melting model presented here suggests that mantle sources for basalts from Taihang Mountains should be greater than 70–80 km deep. Geophysical data also reveal that the current lithospheric thickness in this area is around 80–100 km (Ma, 1989). Fig. 11 illustrates the generation of basaltic magma in the Taihang

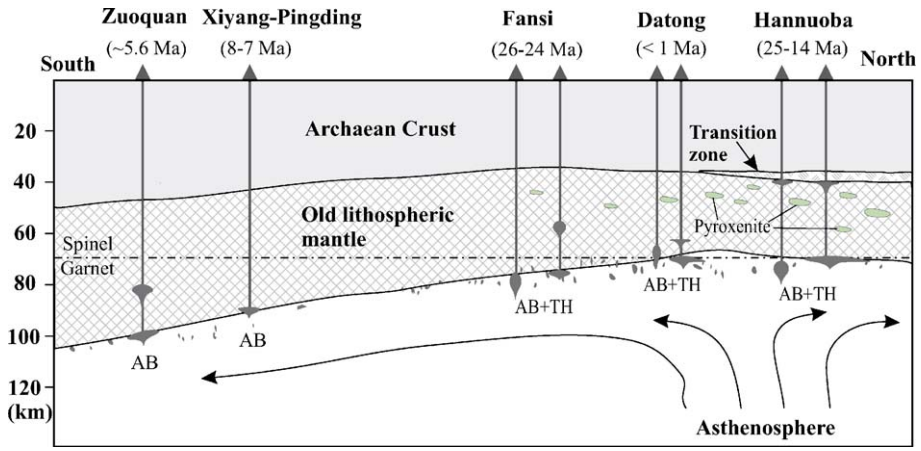

Fig. 11. Sketch map showing the generation of Cenozoic basalts in the Taihang Mountains. The magmas were produced from partial melting of asthenosphere and interaction with lithospheric mantle through thermo-mechanical processes, which were triggered by the continuous upwelling of asthenosphere at continental extension settings. The illustration for the magmatism of Hannuoba and Datong basalts is based on Chen et al. (2001) and Xu et al. (2004, 2005), respectively. AB = alkaline basalt; TH = tholeiite.

Mountains. A Cenozoic tensional regime might reactivate old faults and cracks, which induced the intrusion of initial partial melts and acted as a conduit for transporting magma (hence heat) upwards to raise the ambient temperature of old lithosphere. A progressive erosion of the lithospheric mantle through thermo-mechanical processes with the upwelling of asthenosphere occurred subsequently. Thus, asthenospheric melts with minor involvement of old lithospheric mantle generated these basalts. As mentioned above, the lithosphere beneath the northern North China Craton could be first stretched firstly and then thinned as an effect of continental extension due to the sinistral rotation of Ordos block. Therefore, the upwelling asthenosphere might initiate partial melting first beneath the northern Taihang Mountains (Fig. 11). The lithospheric thickness is smaller on the northern margin of the craton in the Taihang Mountains compared to the center.

The mechanism of lithospheric thinning is still hotly debated. On the basis of the above discussion, we propose that continental collision (India–Eurasia collision) and asthenospheric upwelling might be important mechanisms for triggering the melting of asthenospheric material with/without minor component of old lithospheric mantle.

6. Conclusions

The integrated K–Ar age, elemental and Sr–Nd–Pb isotopic studies on the basalts from Taihang Mountains allow us to draw the following conclusions:

(1) Although the basalts from the Taihang Mountains of the central NCC are definitely OIB-like in trace element patterns and Sr–Nd isotopic compositions, they originated from asthenospheric mantle, rather than a plume source.
(2) Cenozoic basalts from the Taihang Mountains are generated from small degrees of partial melting of asthenosphere, with some contributions of old lithospheric mantle in a continental extensional regime.
(3) Basaltic magmatism and lithospheric evolution in the Taihang Mountains since the Late Eocene may be related to the counterclockwise rotation of the Ordos block and extension along the Shanxi–Shaanxi graben system as a result of the India–Eurasia collision.
(4) Cenozoic lithosphere thickness is inferred to be greater towards the center of the craton compared to the northern margin in the Taihang Mountains.

Acknowledgements

We are grateful to Associate Editor R. L. Rudnick and the two anonymous referees for their constructive reviews that significantly improved the manuscript. Many thanks to Prof. R. L. Rudnick for her considerable time and efforts in reviewing and revising the manuscript, especially in helping with improving the English. This research was financially supported by the Natural Science Foundation of China (grants 40225009, 40534022 and 40503004) and Chinese Academy of Sciences (KZCX3-SW-135). We are also appreciated for their assistance in major, trace elements and isotopic analyses of the State Key Laboratory of Lithospheric Evolution in the IGG. **[RR]**

Appendix A
Analyses of GSR-3 standard by ICP-MS

(ppm)	Meas. $n=2$	1σ	RSD (%)	Ref.	RE (%) (%)	(ppm)	Meas. $n=2$	1σ	RSD (%)	Ref.	RE (%) (%)
Cr	127	16	3.6	134	4.96	Eu	3.10	0.31	2.3	3.2	3.13
Co	44.1	5.2	4.5	46.5	5.16	Gd	8.50	0.70	1.7	8.5	−0.03
Ni	134	11	2.4	140	4.20	Tb	1.15	0.22	2.8	1.2	4.17
Rb	38.2	6.0	3.1	37	−3.29	Dy	5.48	0.36	1.8	5.6	2.23
Sr	1050	100	4.4	1100	4.51	Ho	0.90	0.10	3.0	0.88	−2.04
Y	20.9	5.0	2.6	22	4.97	Er	1.91	0.34	4.6	2	4.50
Zr	265	30	2.7	277	4.28	Tm	0.27	0.10	3.7	0.28	3.57
Nb	70.8	12.1	4.1	68	−4.07	Yb	1.43	0.52	2.1	1.5	4.67
Ba	501	40	4.0	527	4.93	Lu	0.18	0.10	2.7	0.19	3.68
La	53.5	7.5	3.1	56	4.46	Hf	6.80	0.81	1.9	6.5	−4.63
Ce	101	12	2.5	105	3.81	Ta	4.10	0.62	3.2	4.3	4.65
Pr	12.6	1.6	2.2	13.2	4.85	Pb	6.80	4.02	4.0	7	2.86
Nd	52.0	5.0	3.2	54	3.70	Th	6.08	1.23	2.1	6	−1.36

Appendix A (*continued*)

(ppm)	Meas. $n=2$	1σ	RSD (%)	Ref.	RE (%)	(ppm)	Meas. $n=2$	1σ	RSD (%)	Ref.	RE (%)
Sm	9.90	0.70	1.6	10.2	2.94	U	1.34	0.50	3.3	1.4	4.00

n: number of analyses; Meas.: measured value; RSD: relative standard deviation; Ref.: reference value; RE: relative error between measured and recommended values.

Appendix B

Average EMP data for mineral compositions of spinel lherzolite xenoliths from Fansi, North China Craton

Sample	*n*	SiO_2	TiO_2	Al_2O_3	Cr_2O_3	FeO	MnO	MgO	CaO	Na_2O	NiO	Total	Mg#
FS-12 ol	6	41.65	0.03	0.00	0.03	8.75	0.12	49.52	0.07	0.00	0.43	100.6	91.1
FS-26 ol	6	41.07	0.01	0.00	0.05	8.37	0.05	50.67	0.04	0.01	0.32	100.6	91.6
FS-12 opx	4	56.54	0.01	3.18	0.41	5.41	0.13	33.38	0.69	0.08	0.12	99.9	91.7
FS-26 opx	4	55.59	0.11	3.14	0.46	5.16	0.14	34.67	0.59	0.04	0.06	100.0	92.4
FS-12 cpx	6	53.99	0.25	4.98	0.81	2.34	0.06	16.20	19.97	1.24	0.05	99.9	92.6
FS-26 cpx	6	53.82	0.28	4.39	1.16	2.20	0.07	16.44	19.59	0.85	0.03	98.8	93.1
FS-12 sp	2	0.05	0.11	52.53	15.55	9.76	0.08	20.54	0.00	0.00	0.40	99.0	79.1
FS-26 sp	4	0.05	0.08	44.14	9.92	10.46	0.11	20.92	0.01	0.02	0.39	98.9	76.2

n: number of individual spot analyses; Mg# = 100 × molar Mg/(Mg + Fe).

References

Abdel-Rahmann, A.M., 2002. Mesozoic volcanism in the Middle East: geochemical, isotopic and petrogenetic evolution of extension-related alkali basalts from central Lebanon. Geol. Mag. 139, 621–640.

Anders, E., Grevesse, N., 1989. Abundances of the elements: meteoritic and solar. Geochim. Cosmochim. Acta 53, 197–214.

Arndt, N.T., Christensen, U., 1992. The role of lithospheric mantle in continental flood volcanism: thermal and geochemical constraints. J. Geophys. Res. 97, 10967–10981.

Barry, T.L., Kent, R.W., 1998. Cenozoic magmatism in Mongolia and the origin of Central and East Asian basalts. In: Flower, M.F.J., Chung, S.L., Lo, C.H., Lee, T.Y. (Eds.), Mantle Dynamics and Plate Interactions in East Asia. Geodynamics Series, vol. 27. AGU, Washington, pp. 347–364.

Basu, A.R., Wang, J.W., Huang, W.K., Xie, G.H., Tatsumoto, M., 1991. Major element, REE, and Pb, Nd, and Sr isotopic geochemistry of Cenozoic volcanic rocks of eastern China: implications for their origin from suboceanic-type mantle reservoirs. Earth Planet. Sci. Lett. 105, 149–169.

Chen, S.H., O'Reilly, S.Y., Zhou, X.H., Griffin, W.L., Zhang, G.H., Sun, M., Feng, J.L., Zhang, M., 2001. Thermal and petrological structure of the lithosphere beneath Hannuoba, Sino-Korean Craton, China: evidence from xenoliths. Lithos 56, 267–301.

Chen, B., Jahn, B.M., Zhai, M.G., 2004. Petrogenesis of the Mesozoic intrusive complexes from the southern Taihang Orogen, North China Craton: element and Sr–Nd–Pb isotopic constraints. Contrib. Mineral. Petrol. 148, 489–501.

Chung, S.L., Chu, M.F., Zhang, Y., Xie, Y., Lo, C.H., Lee, T.Y., Lan, C.Y., Li, X., Zhang, Q., Wang, Y., 2005. Tibetan tectonic evolution inferred from spatial and temporal variations in post-collisional magmatism. Earth Sci. Rev. 68, 173–196.

Fan, Q.C., Hooper, P.R., 1991. The Cenozoic basaltic rocks of eastern China: petrology and chemical composition. J. Petrol. 32, 765–810.

Fan, W.M., Zhang, H.F., Baker, J., Jarvis, K.E., Mason, P.R.D., Menzies, M.A., 2000. On and off the north China craton: where is the Archaean keel? J. Petrol. 41, 933–950.

Fan, W.M., Guo, F., Wang, Y.J., Lin, G., 2003. Late Mesozoic calc-alkaline volcanism of post-orogenic extension in the northern Da Hinggan Mountains, northeastern China. J. Volcanol. Geotherm. Res. 121, 115–135.

Fan, W.M., Guo, F., Wang, Y.J., Zhang, M., 2004. Late Mesozoic volcanism in the northern Huaiyang tectono–magmatic belt, central China: partial melts from a lithospheric mantle with subducted continental crust relicts beneath the Dabie orogen? Chem. Geol. 209, 27–48.

Flower, M., Tamaki, K., Hoang, N., 1998. Mantle extrusion: a model for dispersed volcanism and Dupal-like asthenosphere in East Asia and the Western Pacific. In: Flower, M.F.J., Chung, S.L., Lo, C.H., Lee, T.Y. (Eds.), Mantle Dynamics and Plate Interactions in East Asia. Geodynamics Series, vol. 27. AGU, Washington, pp. 67–88.

Fraser, K.J., Hawkesworth, C.J., Erland, A.J., Mitchell, R.H., Scott-Smith, B.H., 1985. Sr, Nd and Pb isotope and minor element geochemistry of lamproites and kimberlites. Earth Planet. Sci. Lett. 76, 57–70.

Furman, T., Graham, D., 1999. Erosion of lithospheric mantle beneath the East African rift system: geochemical evidence from the Kivu volcanic province. Lithos 48, 237–262.

Gao, S., Rudnick, R.L., Carlson, R.W., Mcdonough, W.F., Liu, Y.S., 2002. Re–Os evidence for replacement of ancient mantle lithosphere beneath the North China craton. Earth Planet. Sci. Lett. 198, 307–322.

Gao, S., Rudnick, R.L., Yuan, H.L., Liu, X.M., Liu, Y.S., Xu, W.L., Ling, W.L., Ayers, J., Wang, X.C., Wang, Q.H., 2004. Recycling lower continental crust in the North China craton. Nature 432, 892–897.

Gorring, M.L., Kay, S.M., 2001. Mantle processes and sources of Neogene slab window magmas from Southern Patagonia, Argentina. J. Petrol. 42, 1067–1094.

Griffin, W.L., Zhang, A.D., O'Reilly, S.Y., Ryan, C.G., 1998. Phanerozoic evolution of the lithosphere beneath the Sino-Korean

Craton. In: Flower, M.F.J., Chung, S.L., Lo, C.H., Lee, T.Y. (Eds.), Mantle Dynamics and Plate Interactions in East Asia. Geodynamics Series, vol. 27. AGU, Washington, pp. 107–126.

Hart, S.R., 1984. A large scale isotope anomaly in the southern hemisphere mantle. Nature 309, 753–757.

Hofmann, A.W., 1988. Chemical differentiation of the Earth: the relationship between mantle, continental crust, and the oceanic crust. Earth Planet. Sci. Lett. 90, 297–314.

Hofmann, A.W., 1997. Early evolution of continents. Science 275, 498–499.

Hofmann, A.W., Jochum, K.P., Seufert, M., White, W.M., 1986. Nb and Pb in oceanic basalts: new constraints on mantle evolution. Earth Planet. Sci. Lett. 79, 33–45.

Jahn, B.M., Wu, F.Y., Lo, C.H., 1999. Crust–mantle interaction induced by deep subduction of the continental crust: geochemical and Sr–Nd isotopic evidence from post-collisional mafic-ultramafic intrusions of the northern Dabie Complex, Central China. Chem. Geol. 157, 119–146.

Le Bas, M., Le Maitre, R.W., Strekeisen, A., Zanettin, B., 1986. A chemical classification of volcanic rocks based on the total alkali–silica diagram. J. Petrol. 27, 745–750.

Liu, D.Y., Nutman, A.P., Compston, W., Wu, J.S., Shen, Q.H., 1992a. Remnants of 3800 Ma crust in the Chinese part of the Sino-Korean craton. Geology 20, 339–342.

Liu, R.X., Chen, W.J., Sun, J.Z., Li, D.M., 1992b. The K–Ar age and tectonic environment of Cenozoic volcanic rocks in China. In: Liu, R.X. (Ed.), Chronology and Geochemistry of Cenozoic Volcanic Rocks in China. Seismologic Press, pp. 1–43 (in Chinese).

Liu, C.Q., Masuda, A., Xie, G.H., 1994. Major- and trace-element compositions of Cenozoic basalts in eastern China: petrogenesis and mantle source. Chem. Geol. 114, 19–42.

Liu, M., Cui, X., Liu, F., 2004. Cenozoic rifting and volcanism in eastern China: a mantle dynamic link to the Indo-Asian collision? Tectonophysics 393, 29–42.

Liu, Y.S., Gao, S., Lee, C.T.A., Hu, S.H., Liu, X.M., Yuan, H.L., 2005. Melt–peridotite interactions: Links between garnet pyroxenite and high-Mg# signature of continental crust. Earth Planet. Sci. Lett. 234, 39–57.

Ma, X., 1989. Atlas of Active Faults in China, Beijing. Seismologic Press, p. 120.

McDonough, W.F., Sun, S.S., 1995. The composition of the earth. Chem. Geol. 120, 223–253.

McKenzie, D., O'Nions, R.K., 1995. The source regions of oceanic island basalts. J. Petrol. 36, 133–159.

Menzies, M.A., Xu, Y.G., 1998. Geodynamics of the North China Craton. In: Flower, M.F.J., Chung, S.L., Lo, C.H., Lee, T.Y. (Eds.), Mantle Dynamics and Plate Interactions in East Asia. Geodynamics Series, vol. 27. AGU, Washington, pp. 155–165.

Menzies, M.A., Fan, W.M., Zhang, M., 1993. Palaeozoic and Cenozoic lithoprobes and the loss of (120 km of Archaean lithosphere, Sino-Korean craton, China. In: Prichard, H.M., Alabaster, T., Harris, N.B.W., Neary, C.R. (Eds.), Magmatic Processes and Plate TectonicsGeol. Soc. Spec. Publ., vol. 76, pp. 71–81.

Nicholson, H., Latin, D., 1992. Olivine tholeiites from Krafla, Iceland: evidence for variations in the melt fraction within a plume. J. Petrol. 33, 1105–1124.

Peng, Z.C., Zartman, R.E., Futa, K., Chen, D.G., 1986. Pb-, Sr- and Nd-isotopic systematics and chemical characteristic of Cenozoic basalts, eastern China. Chem. Geol. 59, 3–33.

Reisberg, L., Zhi, X., Lorand, J.P., Wagner, C.W., Peng, Z., Zimmermann, C., 2005. Re–Os and S systematics of spinel peridotite xenoliths from east central China: evidence for contrasting effects of melt percolation. Earth Planet. Sci. Lett. 239, 286–308.

Ren, J., Tamaki, K., Li, S., Zhang, J., 2002. Late Mesozoic and Cenozoic rifting and its dynamic setting in eastern China and adjacent areas. Tectonophysics 344, 175–205.

Rudnick, R.L., Gao, S., 2003. Composition of the continental crust. In: Rudnick, R.L., (Ed), The Crust. In: Holland, H.D., Turekian, K.K., (Ed), Treatise on Geochemistry, vol. 3. Elsevier-Pergamon, Oxford. pp. 1–64.

Rudnick, R.L., Gao, S., Ling, W.L., Liu, Y.S., Mcdonough, W.F., 2004. Petrology and geochemistry of spinel peridotite xenoliths from Hannuoba and Qixia, North China Craton. Lithos 77, 609–637.

Rudnick, R.L., Gao, S., Yuan, H.L., Puchtell, I., Walker, R., 2006. Persistence of Paleoproterozoic lithospheric mantle in the Central Zone of the North China Craton. Abstract for the International Conference on Continental Volcanism–IAVCEI.

Shaw, D.M., 1970. Trace elements fractionation during anatexis. Geochim. Cosmochim. Acta 34, 237–243.

Song, Y., Fery, F.A., 1989. Geochemistry of peridotite xenoliths in basalt from Hannuoba, eastern China: implications for subcontinental mantle heterogeneity. Geochim. Cosmochim. Acta 53, 97–113.

Song, Y., Frey, F.A., Zhi, X., 1990. Isotopic characteristics of Hannuoba basalts, eastern China: implications for their petrogenesis and the composition of subcontinental mantle. Chem. Geol. 88, 35–52.

Steiger, R.H., Jager, E., 1977. Subcommission on geochronology; convention on the use of decay constants in geochronology and cosmochronology. Earth Planet. Sci. Lett. 36, 359–362.

Sun, S.S., McDonough, W.F., 1989. Chemical and isotopic systematic of oceanic basalt: implication for mantle composition and processes. In: Saunders, A.D., Norry, M.J. (Eds.), Magmatism in the Oceanic Basins Spec. Publ. Geol. Soc. London, vol. 42, pp. 313–346.

Tang, Y.J., Zhang, H.F., Ying, J.F., 2004. High-Mg olivine xenocrysts entrained in Cenozoic basalts in central Taihang Mountains: relicts of old lithospheric mantle. Acta Petrol. Sin. 20, 1243–1252 (in Chinese with English abstract).

Tatsumoto, M., Basu, A.R., Huang, W.K., Wang, J.W., Xie, G.H., 1992. Sr, Nd, and Pb isotopes of ultramafic xenoliths in volcanic rocks of eastern China: enriched components EMI and EMII in subcontinental lithosphere. Earth Planet. Sci. Lett. 113, 107–128.

Tian, Z., Han, P., Xu, K., 1992. The Mesozoic–Cenozoic East China rift system. Tectonophysics 208, 341–363.

Tu, K., Flower, M.F., Carlson, R.W., Zhang, M., Xie, G.H., 1991. Sr, Nd, and Pb isotopic compositions of Hainan basalts (south China): implications for a subcontinental lithosphere Dupal source. Geology 19, 567–569.

Turner, S., Hawkesworth, C., 1995. The nature of the sub-continental mantle: constraints from the major element composition of continental flood basalts. Chem. Geol. 120, 295–314.

Wang, Y.J., Fan, W.M., Zhang, Y.H., 2004. Geochemical, 40Ar/39Ar geochronological and Sr–Nd isotopic constraints on the origin of Paleoproterozoic mafic dikes from the southern Taihang Mountains and implications for the ca. 1800 Ma event of the North China Craton. Precam. Res. 135, 55–79.

Wang, Y.J., Fan, W.M., Zhang, H.F., Peng, T.P., 2006. Early Cretaceous gabbroic rocks from the Taihang Mountains: implications for a paleosubduction-related lithospheric mantle beneath the central North China Craton. Lithos 86, 281–302.

Wittke, J.H., Mack, L.E., 1993. OIB-like mantle source for continental alkaline rocks of the Balcones province, Texas: trace elements and isotopic evidence. J. Petrol. 101, 333–344.

Wu, Y.S., Wang, X.W., 1978. Recent basalts in Shanxi province. Regional Geological Survey Party, Bureau of Geology of Shanxi Province, pp. 1–136 (in Chinese).

Xie, G.H., Wang, J.W., 1992. The geochemistry of Hannuoba basalts and their ultra-mafic xenoliths. In: Liu, R.X. (Ed.), The Age and Geochemistry of Cenozoic Volcanic Rock in China. Seismologic Press, pp. 149–170 (in Chinese).

Xu, Y.G., 2001. Thermo-tectonic destruction of the Archean lithospheric keel beneath the Sino-Korean Craton in China: evidence, timing and mechanism. Phys. Chem. Earth (A) 26, 747–757.

Xu, Y.G., 2002. Evidence for crustal components in the mantle and constrains on crustal recycling mechanisms: pyroxenite xenoliths from Hannuoba, North China. Chem. Geol. 182, 301–322.

Xu, Y.G., Bodinier, J.-L., 2004. Contrasting enrichments in high- and low- temperature mantle xenoliths from Nushan, Eastern China: results of a single metasomatic event during lithospheric accretion? J. Petrol. 45, 321–341.

Xu, Y.G., Fan, W.M., Lin, G., 1995. Lithosphere–asthenosphere interaction: a comparative study on Cenozoic and Mesozoic basalts around Bohai area. Geotecton. Metallogen. 19, 1–13.

Xu, Y.G., Chung, S.L., Ma, J.L., Shi, L.B., 2004. Contrasting Cenozoic lithospheric evolution and architecture in the western and eastern Sino-Korean craton: constrains from geochemistry of basalts and mantle xenoliths. J. Geol. 112, 593–605.

Xu, Y.G., Ma, J.L., Frey, F.A., Feigenson, M.D., Liu, J.F., 2005. Role of lithosphere–asthenosphere interaction in the genesis of Quaternary alkali and tholeiitic basalts from Datong, western North China Craton. Chem. Geol. 224, 247–271.

Ye, H., Zhang, B.T., Ma, F., 1987. The Cenozoic tectonic evolution of the great North China: two types of rifting and crustal necking in the great North China and their tectonic implications. Tectonophysics 133, 217–227.

Zhang, H.F., 2005. Transformation of lithospheric mantle through peridotite–melt reaction: a case of Sino-Korean Craton. Earth Planet. Sci. Lett. 237, 768–780.

Zhang, H.F., 2006. Peridotite–melt interaction: an important mechanism for the compositional transformation of lithospheric mantle. Earth Science Frontiers 13, 65–75 (in Chinese with English abstract).

Zhang, M., Zhou, X.H., Zhang, J.B., 1998a. Nature of the lithospheric mantle beneath NE China: evidence from potassic volcanic rocks and mantle xenoliths. In: Flower, M.F.J., Chung, S.L., Lo, C.H., Lee, T.Y. (Eds.), Mantle Dynamics and Plate Interactions in East Asia. Geodynamics Series, vol. 27. AGU, Washington, pp. 197–219.

Zhang, Y.Q., Mercier, J.L., Vergély, P., 1998b. Extension in the graben systems around the Ordos (China), and its contribution to the extrusion tectonics of south China with respect to Gobi–Mongolia. Tectonophysics 285, 41–75.

Zhang, H.F., Menzies, M.A., Gurney, J.J., Zhou, X.H., 2001. Cratonic peridotites and silica-rich melts: diopside–enstatite relationships in polymict xenoliths, Kaapvaal, South Africa. Geochim. Cosmochim. Acta 65, 3365–3377.

Zhang, H.F., Sun, M., Zhou, X.H., Fan, W.M., Zai, M.G., Ying, J.F., 2002. Mesozoic lithosphere destruction beneath the North China Craton: evidence from major-, trace-element and Sr–Nd–Pb isotope studies of Fangcheng basalts. Contrib. Mineral. Petrol. 144, 241–253.

Zhang, H.F., Sun, M., Zhou, X.H., Zhou, M.F., Fan, W.M., Zheng, J.P., 2003a. Secular evolution of the lithosphere beneath the eastern North China Craton: evidence from Mesozoic basalts and high-Mg andesites. Geochim. Cosmochim. Acta 67, 4373–4387.

Zhang, Y., Ma, Y., Yang, N., Shi, W., Dong, S., 2003b. Cenozoic extensional stress evolution in North China. J. Geodyn. 36, 591–613.

Zhang, H.F., Sun, M., Zhou, M.F., Fan, W.M., Zhou, X.H., Zhai, M.G., 2004. Highly heterogeneous late Mesozoic lithospheric mantle beneath the north China Craton: evidence from Sr–Nd–Pb isotopic systematics of mafic igneous rocks. Geol. Mag. 141, 55–62.

Zhao, G.C., Cawood, P.A., Wilde, S.A., Sun, M., 2000. Metamorphism of basement rocks in the Central Zone of the North China craton: implications for Paleoproterozoic tectonic evolution. Precam. Res. 103, 55–88.

Zhao, G.C., Wilde, S.A., Cawood, P.A., Sun, M., 2001. Archean blocks and their boundaries in the North China Craton: lithological, geochemical, structural and P–T path constraints and tectonic evolution. Precam. Res. 107, 45–73.

Zheng, J.P., O'Reilly, S.Y., Griffin, W., Lu, F.X., Zhang, M., Pearson, N., 2001. Relict refractory mantle beneath the eastern North China block: significance for lithosphere evolution. Lithos 57, 43–66.

Zhi, X.C., Qin, X., 2004. Re–Os isotope geochemistry of mantle-derived peridotite xenoliths from eastern China: constraints on the age and thinning of lithosphere mantle. Acta Petrol. Sin. 20, 989–998 (in Chinese with English abstract).

Zhi, X.C., Song, Y., Frey, F.A., Feng, J.L., Zhai, M.Z., 1990. Geochemistry of Hannuoba basalts, eastern China: constraints on the origin of continental alkalic and tholeiitic basalt. Chem. Geol. 88, 1–33.

Zhou, X.H., Armstrong, R.L., 1982. Cenozoic volcanic rocks of eastern China-secular and geographic trends in chemistry and strontium isotopic composition. Earth Planet. Sci. Lett. 58, 301–329.

Zhou, X.H., Sun, M., Zhang, G.H., Chen, S.H., 2002. Continental crust and lithospheric mantle interaction beneath North China: isotopic evidence from granulite xenoliths in Hannuoba, Sino-Korean craton. Lithos 62, 111–124.

Zindler, A., Hart, S.R., 1986. Chemical geodynamics. Annu. Rev. Earth Planet. Sci. 14, 493–571.

Zou, H.B., Zindler, A., Xu, X.S., Qi, Q., 2000. Major, trace element, and Nd, Sr and Pb isotope studies of Cenozoic basalts in SE China: mantle sources, regional variations, and tectonic significance. Chem. Geol. 171, 33–47.

Zou, H.B., Reid, M.R., Liu, Y.S., Yao, Y.P., Xu, X.S., Fan, Q.C., 2003. Constraints on the origin of historic potassic basalts from northeast China by U–Th disequilibrium data. Chem. Geol. 200, 189–201.